A Malaria Diagnostic System Based on Electric Impedance Spectroscopy

by

Sungjae Ha

B. Eng. Electrical Engineering
Pohang University of Science and Technology, 2009

SUBMITTED TO THE DEPARTMENT OF ELECTRICAL ENGINEERING AND COMPUTER SCIENCE IN PARTIAL FULFILLMENT OF THE REQUIREMENTS FOR THE DEGREE OF

MASTER OF SCIENCE IN ELECTRICAL ENGINEERING AND COMPUTER SCIENCE

AT THE

MASSATCHUSETTS INSTITUTE OF TECHNOLOGY

JUNE 2011

Signature of author: _____
Department of Electrical Engineering and Computer Science
May 20, 2011

Certificated by: _____
Anantha P. Chandrakasan
Joseph F. and Nancy P. Keithley Professor of Electrical Engineering
Thesis Supervisor

Accepted by: _____
Leslie A. Kolodziejski
Professor of Electrical Engineering
Chair, Department Committee on Graduate Students

A Malaria Diagnostic System Based on Electric Impedance Spectroscopy

by

Sungjae Ha

Submitted to the Department of Electric Engineering and Computer Science
on May 20, 2011 in Partial Fulfillment of the
Requirements for the Degree of Master of Science in
Electrical Engineering and Computer Science

ABSTRACT

Malaria caused by Plasmodium falciparum infection is one of the major threats to world health and especially to the community without proper medical care. New approach to cost-efficient, portable, miniaturized diagnostic kit is needed. This work explores electric impedance spectroscopy (EIS) on a microfluidic device as a means of malaria diagnosis. This work introduces a microfabricated probe with microfluidic channel, and a high speed impedance analyzer circuit board. Combination of microfluidic device and circuit board resulted in a small-sized EIS system for micro-particles such as human red blood cell (RBC). After invasion by the parasites, RBC undergoes physiological changes including electrical property of cytoplasm and membrane. Detection of infected RBC is demonstrated as well as differentiation of micro-beads by surface charge density using EIS-based diagnostic system. Diagnosis based on EIS has merits over other diagnostic methods since it is label-free and quantitative test and applicable to whole blood, and also the test does not need bulky optical and electrical equipments.

Thesis Supervisor: Anantha P. Chandrakasan
Title: Joseph F. and Nancy P. Keithley Professor of Electrical Engineering

Acknowledgments

I would first like thank my family, especially to my mother, my sister, and my father in heaven. They have been the most precious ones in my life, and they have always been on my side being my energy source and sometimes a comforting shelter. I would like to thank my advisor Prof. Anantha Chandrakasan. Without his care and patience, I would not be able to conduct my research after a great loss. He also reached out to premier researchers in malaria and microfluidics fields for me to learn and do interdisciplinary work. I also appreciate the dear students of ananthagroup who spent days and nights with me for a long time. And Margaret, our administrative assistant, who is always doing so much for all of us. I thank Dr. Sung Jae Kim who helped a lot when I struggled stepping in a new academic field. I gratefully acknowledge Nanomechanics group and Micro/Nanofluidic BioMEMS group at MIT, especially Prof. Subra Suresh and Prof. Jongyoon Han for allowing me to use their lab places. It has been a great joy for me to collaborate with wonderful people there. Analog Device Inc. provided chip samples used in this study, and I appreciate them a lot. I also thank Korean Catholic Community in Boston which has been a big part of my life at MIT and helped me stay cheerful and strong-minded for past two years. I cannot mention every single name, but my dear friends truly believed in me and supported me from deep down in their heart. No words would be enough, but I truly appreciate all of them.

Contents

List of Figures

List of Tables

Chapter 1

Introduction

1.1. Impact of Malaria on Global Health

Malaria is a parasitic disease which infects human red blood cells (RBCs), and it is life-threatening unless treated immediately. Though malaria is preventable and curable, the disease prevails mainly in the countries where there are lack of proper medical facilities, killing about a million people worldwide a year [1].

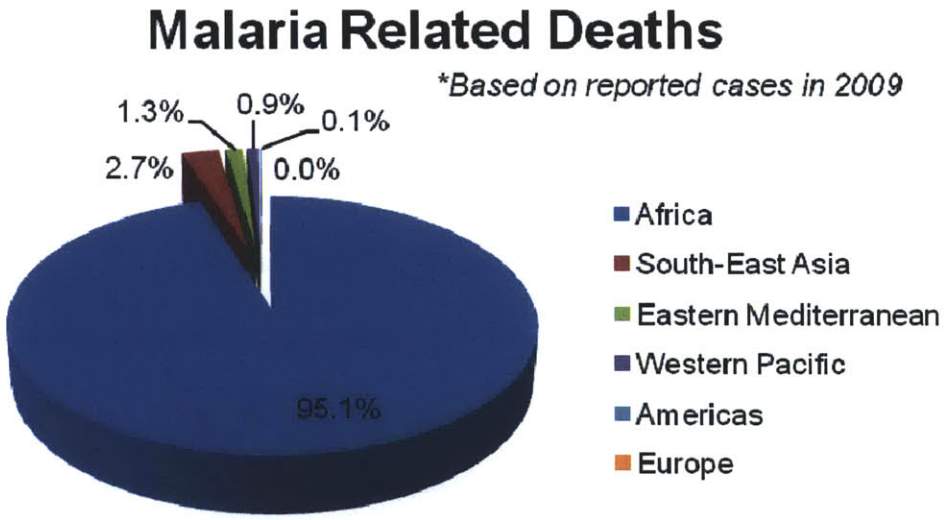

Figure 1. Regional distribution of malaria-related deaths in 2009

Scrutinizing the losses, 95% of malaria deaths reported in 2009 occurred in Africa (Figure 1) and most of them were children. Human immunity developed among adults in the endemic areas over years of exposure reduces the risk that malaria infection will cause severe disease. However, young children with low immunity are at serious risk. For this reason, malaria causes a great number of childhood deaths in Africa, it fact a fifth of total childhood deaths. Although human loss is uncountable, the economic loss in Africa due to the disease is estimated as $12 billion every year [2]. The health cost of malaria including both personal and public expenditures on prevention and treatment in Africa varies between countries. Particularly in some heavy-burden countries, the disease accounts for up to 40% of public health expenditures, 30% ~ 50% of inpatient hospital admissions, and up to 60% of outpatient health clinic visits [3].

World Health Organization claims that early diagnosis and treatment of malaria prevents deaths and reduces malaria transmission. However, the first symptoms, such as fever, headache, chills and vomiting, may be mild and difficult to recognize as malaria [3]. Incorrect diagnosis and treatment can lead to drug resistance of malaria parasites and loss of disease control. It has happened before with chloroquine and sulfacoxine-pyrimethanmine. Thus, the best available treatment, particularly for *P. falciparum* malaria, artemisinin-based combination therapy (ACT) may not be effective to control the disease in the future. Therefore, parasite-based diagnosis in early stage is highly in demand.

1.2. Methods and Issues of Malaria Diagnosis

Various types of diagnostic tests are available (Figure 2), but drawbacks exist in practical applications.

The standard diagnosis of malaria is a microscopic test. Since malaria parasites are visible, optical examination of infected RBC is direct diagnosis of malaria. Once blood sample is collected, a medical expert can stain and examine it under microscope. A Giemsa-stained thick blood film (G-TBF) is usually used to screen for the presence of parasites quickly [4], and 100 fields of G-TBF can screen approximately 1,300,000 RBCs in 0.25μl of whole blood. The process of G-TBF is easy, but it always requires experienced personnel, a microscope, and the chemical dye.

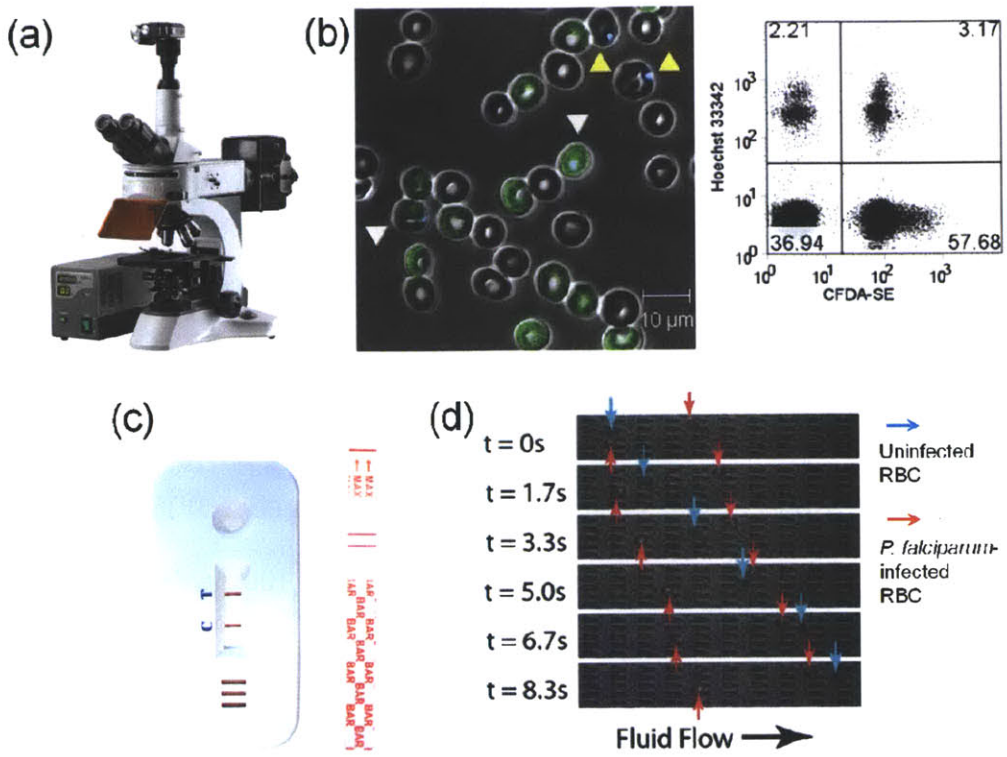

Figure 2. Current diagnostic methods:
(a) G-TBF microscopic test, (b) fluorescent flow cytometry, (c) antigen-based rapid diagnostic test and (d) deformability-based flow cytometry [18].

With automated machines, fluorescent flow cytometry does the same job as the standard test. After fluorescent chemical is attached to the infected RBCs, automated microscope can count the number of infected cells found optically. Similar to G-TBF method, larger sample volume reduces the chance of missing infected cells. After checking millions of erythrocytes, red blood cells, medical personnel can determine that the blood sample is a negative case. Flow cytometry reduces human labors in the repeated examinations of blood. However, the diagnostic time is not very short as the sample preparation and equipment setup

time is added in reality. Another drawback, which is critical, is that automated flow cytometer costs a lot and consumes large amount of energy.

In summary, microscopic test and flow cytometry require experienced personnel and microscopes which are hard to transport to very remote areas. These optical methods can also take long time to examine enough volume of blood sample to find infected RBCs at early stage when parasitemia, the presence of parasites in the blood, is very low as shown in Table 1. Therefore, rapid diagnostic tests are getting popular in the area where a large number of suspected malaria patients reside but there are not many well-organized medical facilities.

Rapid diagnostic tests (RDTs) are able to test a blood sample within an hour or less. The test kits detect special proteins, antigens, produced by parasites, utilizing antigen-antibody reaction. Two common antigens are histidine-rich protein 2 (HRP-2) and lactate dehydrogenase from malaria parasites (pLDH). The test kits are usually as simple as commercial pregnancy test kits. Depending on products, the selectivity and sensitivity to parasites vary. The cost, however, is

Table 1. Parasitemia and clinical correlates [4]

Parasitemia	Parasites/μl	Clinical Correlation
0.0001-0.0004%	5-20	Sensitivity of thick blood film test
0.002%	100	Patients may have symptoms below this level, where malaria is seasonal.
0.2%	10,000	Level above which immunes show symptoms
2-5%	100,000-250,000	Hyperparasitaemia/ severe malaria, increased mortality.
10%	500,000	Exchange-transfusion may be considered/ high mortality

mostly high, so not many patients in malaria-prevalent areas can afford RDT unless supported [4]. Though there are the issues of cost and sensitivity, antigen-based RDT still seems to be an attractive alternative thanks to its size and speed of diagnosis. But it is a qualitative test that cannot give information of how high the parasitemia is and of pathological stage of malaria parasites.

Malaria diagnosis based on the mechanical property of RBC is also proposed. [18] explored microfabricated deformability-based flow cytometry and showed the possibility to detect early state *P. falciparum*-infected RBC within abundant uninfected RBCs. Blood flow in a channel with microfabricated obstacles showed that the average velocities of uninfected RBCs and of infected RBCs are significantly different. However, significant overlap in terms of their dynamic deformability degraded sensitivity of the test. In addition to the sensitivity issue, the test requires video recording of microscopic view, which means it needs microscope, camera, and high computing power. Though deformability-based flow cytometry introduced another approach, more study is still desired.

It is important to take into account that many of malaria-prevalent areas are limited in medical experts, electricity, and proper equipments for medical care. Considering the circumstance, another effective rapid diagnostic tool thus should be investigated to reach out to the resource-limited areas. In this study, microfluidic electric impedance spectroscopy (EIS) is investigated as an alternative approach to malaria diagnosis. The proposed method electrically detects infected cells within a microfluidic device, so it can have advantages over

Table 2. Summary of malaria-diagnostic methods

Method	Characteristics
Giemsa-stained Thick Blood Film (G-TBF)	+ Low cost, easy, standard method - Requires experienced personnel, microscope
Fluorescent flow cytometry	+ Automated test - Requires expensive equipment - Pre-process of sample
Antigen-based Rapid Diagnostic Test (RDT)	+ Easy and fast diagnosis - Qualitative test ◦ Sensitivity and cost vary depending on product.
Deformability-based flow cytometry	- Low sensitivity - Requires video analysis

other diagnostic tests. First, it does not require optical equipments such as microscope, camera, or flow cytometer. Second, it is a quantitative test which gives parasitemia information. Third, the device for this method can be very small in size so that transportation to remote areas is possible. Forth, the device can be as low power as solar- or battery-powered with low power IC design. Fifth, EIS is a label-free analysis which does not require extensive pre-process on the target sample. Lastly, the manufacturing cost can be very low, thank to the grown IC fabrication business.

Chapter 2 and 3 describe the method more in detail.

Chapter 2

Background

This chapter reviews previous works as background for the EIS-based malaria diagnostic system which will be introduced in the following chapter.

2.1. Pathology of Malaria

The cause of malaria is *Plasmodium* parasites. There are four types of *Plasmodium* which infect human among more than 120 species. *Plasmodium falciparum* is the most common, causing more than 90% of the deaths, while *P. vivax* is geographically more widespread. *P. ovale* and *P. malariae* are the other two but far less common.

Mosquito in endemic area is the media of parasite. A bite of an infected female mosquito transfers a few hundreds of sporozoites and one or two of them infect the liver cells, or hepatocytes, within hours. Within 2 weeks, the parasite has produced thousands of daughter merozoites in a single liver cell. As cell bursts, the infective merozoites flow into the bloodstream beginning the rapid asexual replication (binary fission of malaria parasite) as well as invasion of erythrocytes or red blood cells. Inside erythrocytes, the parasite produces 16 to 32

daughters by binary nuclear fissions, and they are released when the red blood cell bursts. Released parasites continue to infect other red blood cells [5].

The symptoms of malaria such as fever, sweats, rigors, chills and even coma and death are related to the reproduction of infected RBCs. A newly infected erythrocyte comes through three stages: a ring stage, a trophozoite stage and a schizont stage. At the schizont stage, the cell releases merozoites. These stages can be optically examined as shown in Figure 3.

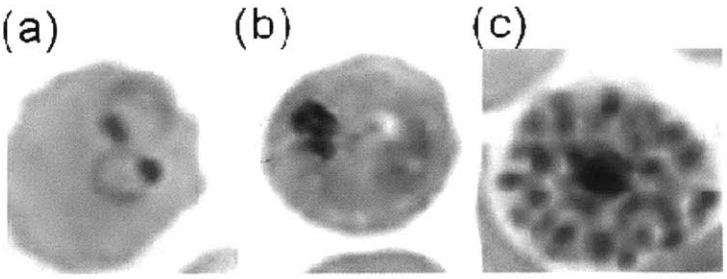

Figure 3. Three stages of *P. falciparum*-infected RBC [5]:
(a) Ring stage. (b) Trophozoite stage. (c) Schizont stage.

After the parasites take up Giemsa stain, the ring stage is the most commonly seen (Figure 4). The parasite cytoplasm forms an incomplete ring. Chromatin, a part of the parasite nucleus, is usually round in shape and stains a deep red. The trophozoite stage is a growing stage, so the parasite within the red blood cell may vary in size from small to quite large. Malaria pigment (hemozoin), a by-product of the growth or metabolism of the parasite, appears as the parasite grows. The pigment has own color ranging from pale yellow to dark brown. At the schizont stage, the malaria parasite starts asexual reproduction. Parasites with a number of chromatin dots and definite cytoplasm can be seen at this stage.

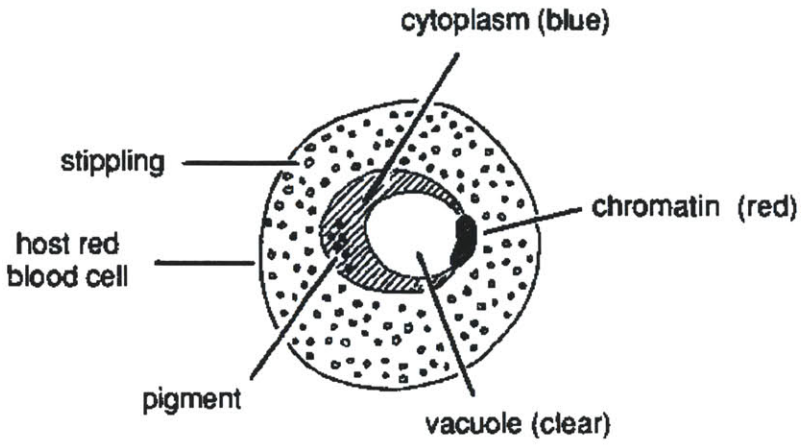

Figure 4. Illustration of a malaria parasite in a host red blood cell

While *P. falciparum* develops in host RBC, RBC undergoes pathological modifications. Parasites consume hemoglobin and form biocrystal called hemozoin, or malaria pigment [5]. During the process, cytoplasm and membrane of RBC change: optical property such as refraction index [6], mechanical property such as membrane fluctuation [6] and cell deformability [18], magnetic susceptibility [7], and also electrical property classified as cell impedance [8]. Among those physiological changes, EIS-based test focuses on the electrical property change.

2.2. Biological Cell Impedance Analysis

A biological cell has its membrane and cytoplasm, and each of them has electric conductance and capacitance. Thus, biological cell can be modeled as a circuit, or a network of passive elements, and even a simplified circuit model can represent its electrical property well [9]. Figure 5a depicts a simple circuit model for RBC and its concordant transfer function to measured data. Using the impedance information of cells, cells can be sorted by their types. Immobilizing cells between the microfabricated electrodes, they differentiated fish red blood cell and

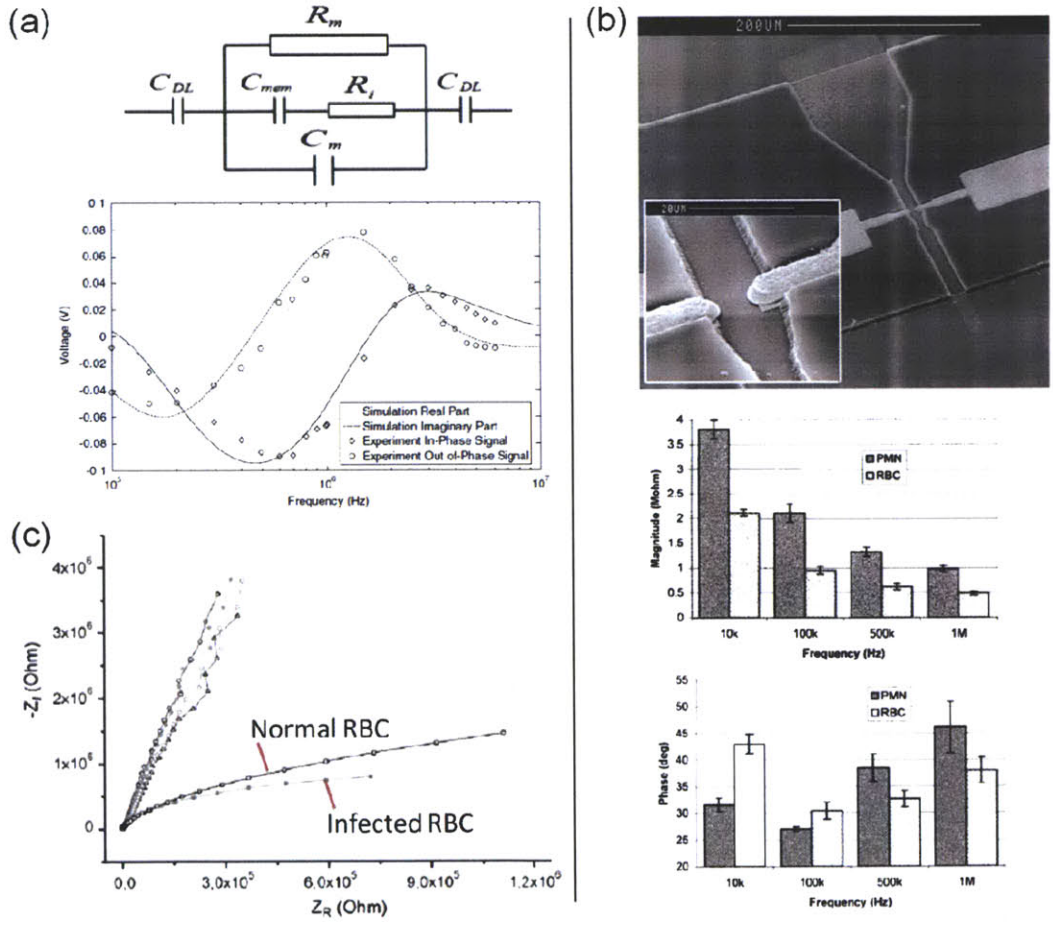

Figure 5. Impedance analysis of immobilized biological cell: (a) equivalent circuit model for RBC [9], (b) cell differentiation by impedance measurement [10] , (c) Nyquist plot showing the impedance change after parasite invasion [8].

human leukocyte which are similar in size [10]. Figure 5b shows microfabricated channel with electrodes (top) and magnitude (middle) and phase (bottom) of impedance of target cells. Impedance analysis of biological cells can also detect physiological change of a single red blood cell after invasion by malaria parasites [8]. To survive within a red blood cell, the malaria parasite alters the permeability of the host's plasma membrane to accomplish nutrient uptake and disposal of waste products. Thus, in addition to hemoglobin consumption [19], the parasites perturb the ionic composition of its host cell [11] resulting changes in the film resistance, rendering the cellular layer less insulating. Figure 5c is Nyquist plot for impedance of a trapped RBC showing that a significant change is observed after invasion by *P. falciparum*.

These studies suggest cell impedance analysis as a possible mean to diagnose malaria. However, other disease can also impact impedance of RBC. Unless other possibilities are ruled out, the result of cell impedance analysis can only give supplementary information about RBC. Low throughput of the method used in [8] also limits the feasibility of the impedance analysis as a diagnostic test. Trapped cell impedance spectroscopy demands lots of effort by an expert, taking long time to investigate each cell. Recalling that malaria parasitemia reaches up only to 10% in severe malaria and it is far less than that in the earlier or mild stages, it can take impractically long to find 10 infected RBC in a million. Thus, the small throughput highly limits the practicality of trapped cell impedance analysis unless time and efforts for diagnosis are unlimited.

2.3. Microfluidic Impedance Spectroscopy

To perform impedance analysis on single cell with high throughput, microfluidic impedance spectroscopy has been studied for many years. While various designs have been studied [20], underlying physics is mostly similar as shown in Figure 8. An impedance analyzer equipment continuously measures electric impedance of a pair of electrodes spaced apart, facing each other or in parallel, in a fluidic channel. When a cell or particle passes between the electrodes, the equipment measures the impedance of the cell or particle in parallel and series to the medium of channel. Since the measurement is conducted in flowing condition, throughput can drastically increase relative to trapped-cell analysis.

The Coulter counter [21], named after its inventor, is the first device that demonstrated the concept of counting flowing cells by impedance measurement.

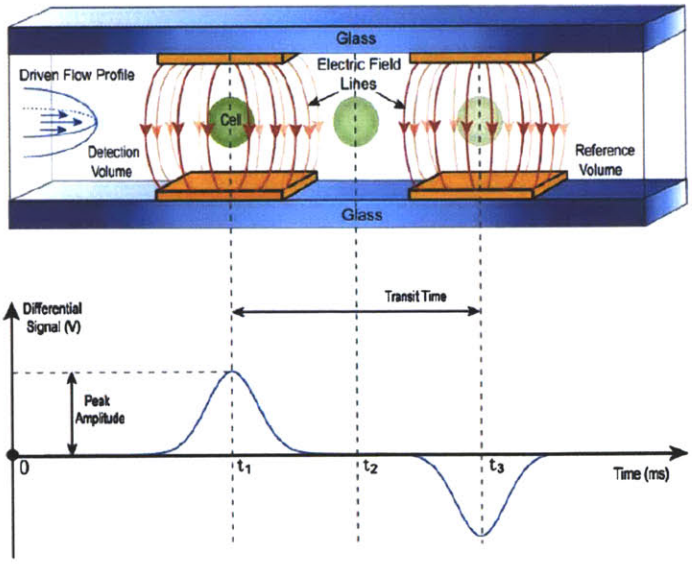

Figure 6. Microfluidic impedance spectroscopy technique [12].

Illustrated in Figure 7, the device measures DC current which is reduced when a less conductive particle blockades the fluidic channel, and count and/or size individual particles. However, DC resistance measurements could only provide size information assuming known conductivity of particle and medium.

Afterwards, a number of microfabricated Coulter counters and its innovations have followed with increased sensitivity to smaller biological targets and higher throughput. Applications include spermatozoa counter chip [13] which has a microfluidic channel of 38μm width and 18μm depth with two 200 nm thick and 20μm wide platinum electrodes. Measuring impedance at 96 kHz to take into account the double layer capacitance between electrodes and fluid medium and the parasitic capacitance, the device is capable of differentiation of small cells in semen by their size. By adding micro-beads, whose size is different from the

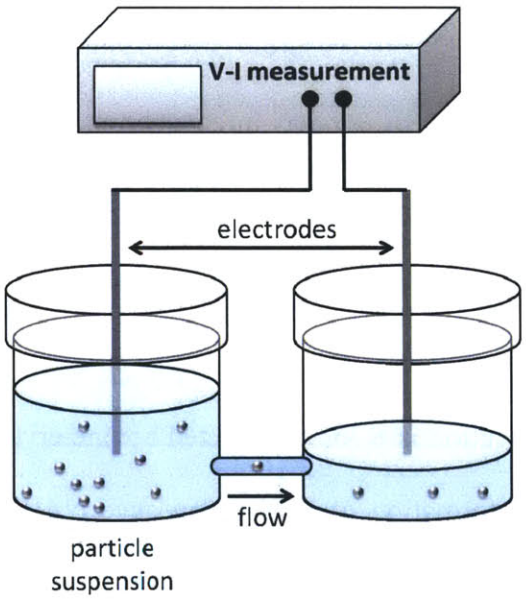

Figure 7. Illustration of the Coulter counter: electric DC current is reduced as a particle or a cell passes through, so that they can be counted and sized.

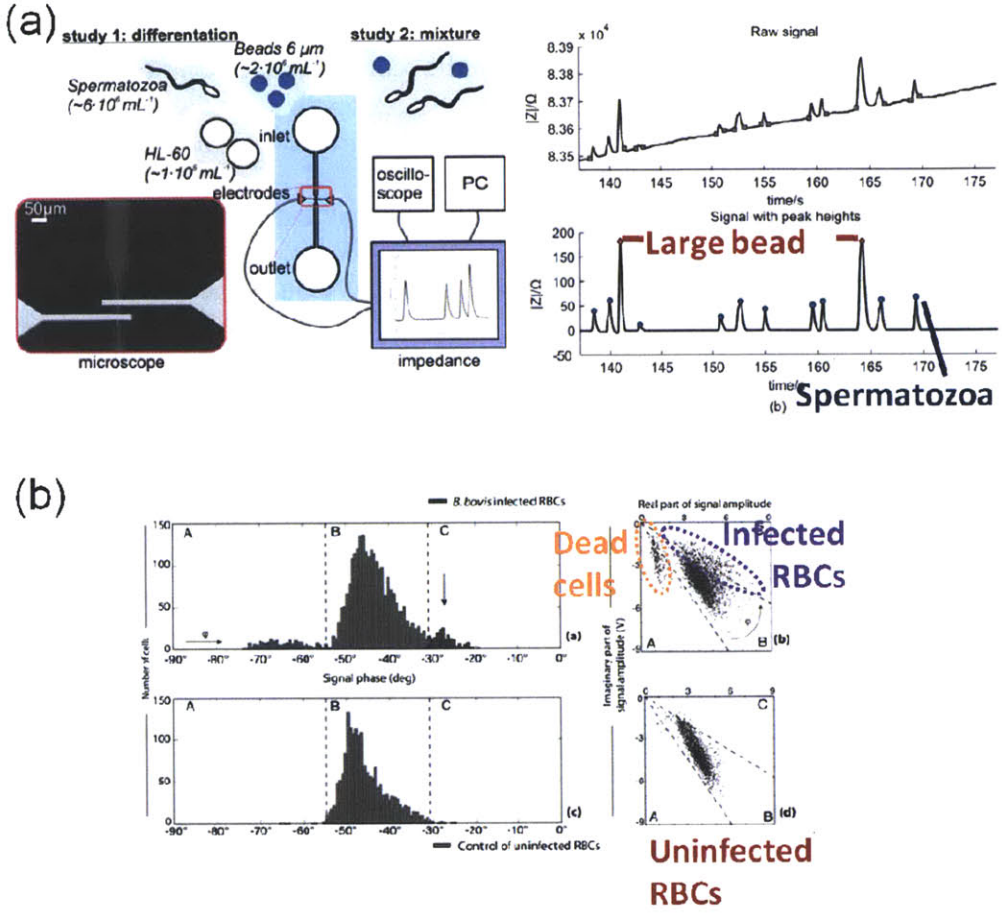

Figure 8. Applications of microfluidic impedance spectroscopy: (a) spermatozoa counter chip [13] and (b) *B. bovis*-infected bovine RBC detection [14].

spermatozoon, of known concentration into the semen sample, it can measure spermatozoon concentration from the ratio of spermatozoon count and bead count in the mixture.

Another application is *B. bovis* infected bovine erythrocyte detection chip utilizing the phase information of RBC impedance [14]. Using high frequency electric impedance spectroscopy, the intracellular property is probed. As the parasites modify the electrical properties of host cells, the infected red blood cells can express phase shift of impedance. Obtained from EIS measurement on

thousands of cells, Figure 8b shows the histogram and scatter plots of the mixed sample and uninfected blood sample. However, the detection method proposed in this work may not be label-free. The work did not account for the effects of fluorescent dyes for visual inspection of infected cell. Fluorescent label may have affected the impedance of the infected cells and that might have shown up in phase shift.

Chapter 3

Proposed Solution and Methods

3.1. Microfluidic EIS-based diagnostic test

This work proposes a new malaria diagnostic test based on electric impedance spectroscopy. A MEMS-IC hybrid system is designed to conduct single cell analysis over millions of RBCs with high speed electronics. The proposed system illustrated in Figure 9 consists of a microfluidic probe device and a data collecting electronics. On the MEMS side, blood sample is injected to the device and then RBCs flow along narrowing microfluidic channel. The electronic part of the system continuously measures the electric impedance of

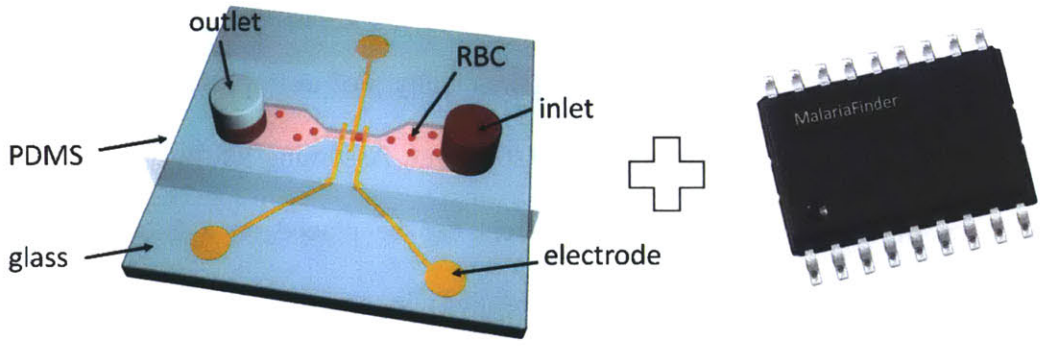

Figure 9. Proposed malaria diagnostic system utilizes microfluidics and electronics.

microfluidic channel with or without red blood cells passing through. Malaria can be diagnosed based on gathered impedance data of red blood cells from whole blood without labeling chemicals.

This approach can results in great reduction in manufacturing cost of rapid diagnostic test kits, since detection of infected RBC does not rely on any chemical reaction which usually raises production and research and development cost. Moreover, the microfluidic part made of transparent material for visual observation at research level can be made of opaque plastic material for consumer products lowering the cost. Besides, the size of EIS-based RDT can be smaller than commercial antigen-based RDT, and EIS technique does not require optical equipment which is usually bulky and heavy. Therefore, this small test kit can easily access to very remote areas and can be even more useful.

However, speed of the system would be slow in single channel system. Assuming that flow rate of 10 nl/min and 50x diluted whole blood is prepared, then it takes 1000 minutes to detect 0.0001% parasitemia. Once single channel system functions correctly, the diagnostic speed can be increased by multiplexing microfluidic channels. Multiplexing is one of the greatest merits of microfluidic system, which can increase throughput drastically. For example, a single-channel microfluidic system has active area of 0.04 mm^2. Assuming 900% space margins between the single channels, 50 channels can be placed on a 2 cm by 1 cm microfluidic device. By putting fifty replicas in one chip, the result is in 20 minutes. Therefore, microfluidic EIS-based malaria diagnostic system can be a possible solution for developing an effective malaria diagnostic device.

3.2. Design of Microfluidic Device

3.2.1. Description of Function

MEMS part of the system is a micro-scale probe to measure electrical property of tiny biological cell. Basically, the probe is a pair of metal electrodes in which a RBC can reside between. To guide blood cells to pass through the space between two electrodes, microfluidic channel is fabricated and accurately placed on the electrodes.

Dimensions of microfluidic channel and electrodes are carefully tested and chosen to investigate each cell at a time and to achieve enough sensitivity to tiny (<10μm in diameter) human RBC. Figure 10 depicts active region of the MEMS device consisting of a microfluidic channel and micro-electrodes.

Microfluidic channel dimension is determined to 30μm x 5μm x 160μm. Cross-sectional area of the channel is fit to RBCs so that the cell flows without much of flow resistance. With this design, cells have to be as small as the height

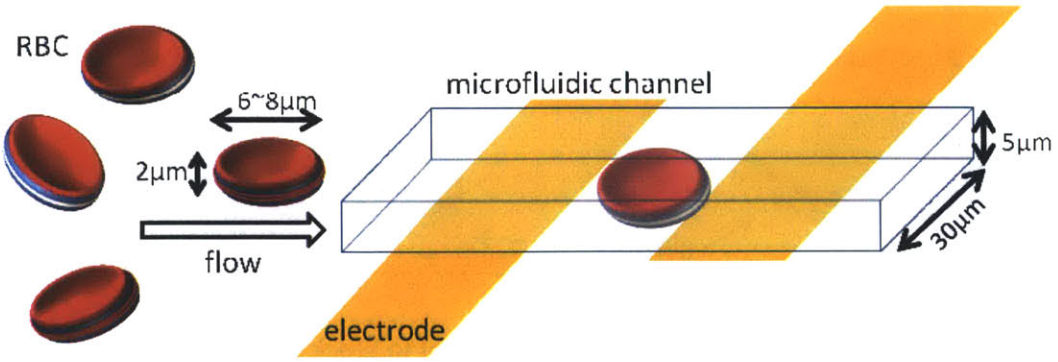

Figure 10. Illustration of microfluidic channel with a pair of electrodes.

of the channel or disk-shaped like RBC to flow into the device. Other large particles or cells such as leukocyte will be filter at the inlet. Length of the channel accommodates three electrodes with 10μm margin. The longer channel eases the alignment; however, it increases fluidic resistance of the channel and high fluid pressure to overcome the fluidic resistance can cause breakage of the device. Therefore, microfluidic channel width is designed to wide except the active region of the microfluidic channel with electrodes.

There is a constraint in the wide microfluidic channel design. Since the depth of channel is only ~5um but width is 200 times of that, PDMS ceiling of channel can easily attach to the bottom glass substrate as shown in Figure 11. To support the ceiling, 40 μm by 40 μm square-shaped pillars were placed with 80 μm spacing.

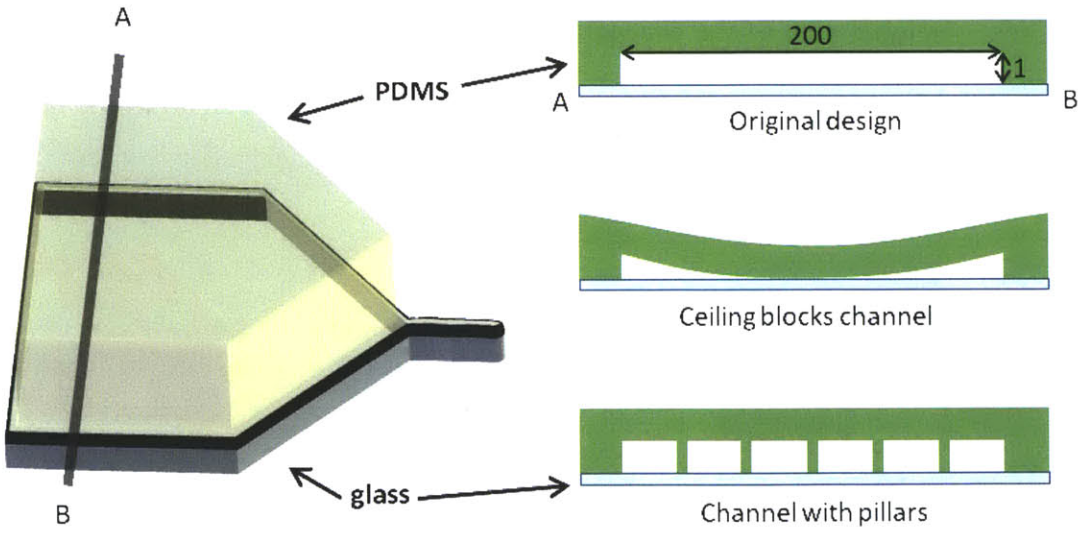

Figure 11. Pillars support ceiling not to block the channel.

Though a pair of electrodes is required for the given impedance converter, three electrodes are drawn first to ease alignment of PDMS cell and glass substrate, and second to utilize the third electrode in future application such as differential sensing of impedance change. The width of and space between electrodes are 20 μm. To make it smaller or larger causes alignment problems or degrades sensitivity of probes, respectively. Length of electrodes is elongated to have alignment margin over the width of microfluidic channel. Electrodes of outer of the active area have width of 1mm. Titanium and gold are used for material of electrodes. Thickness of gold layer is 100 nm to ensure low series resistivity. 10nm-thick titanium layer is used to help adhesion between gold and glass.

3.2.2. Fabrication Process

Figure 12 shows the overall process of microfluidic device fabrication and every step is conducted at TRL in MTL, MIT. While photopatternable silicon (PPS) and an epoxy-based negative photoresist (SU-8) are widely used in microfluidic device fabrication in growing phase, standard silicon photolithography and reactive ion etching process are applied in this study. PPS and SU-8 are preferable methods to make patterns on wafer since they require fewer fabrication steps without silicon etching process. However, the resolutions are limited to ~10μm and ~6μm, respectively [22]. In this study, standard photolithographical techniques are applied to achieve higher resolution, better control on the depth of microchannel, and better yield.

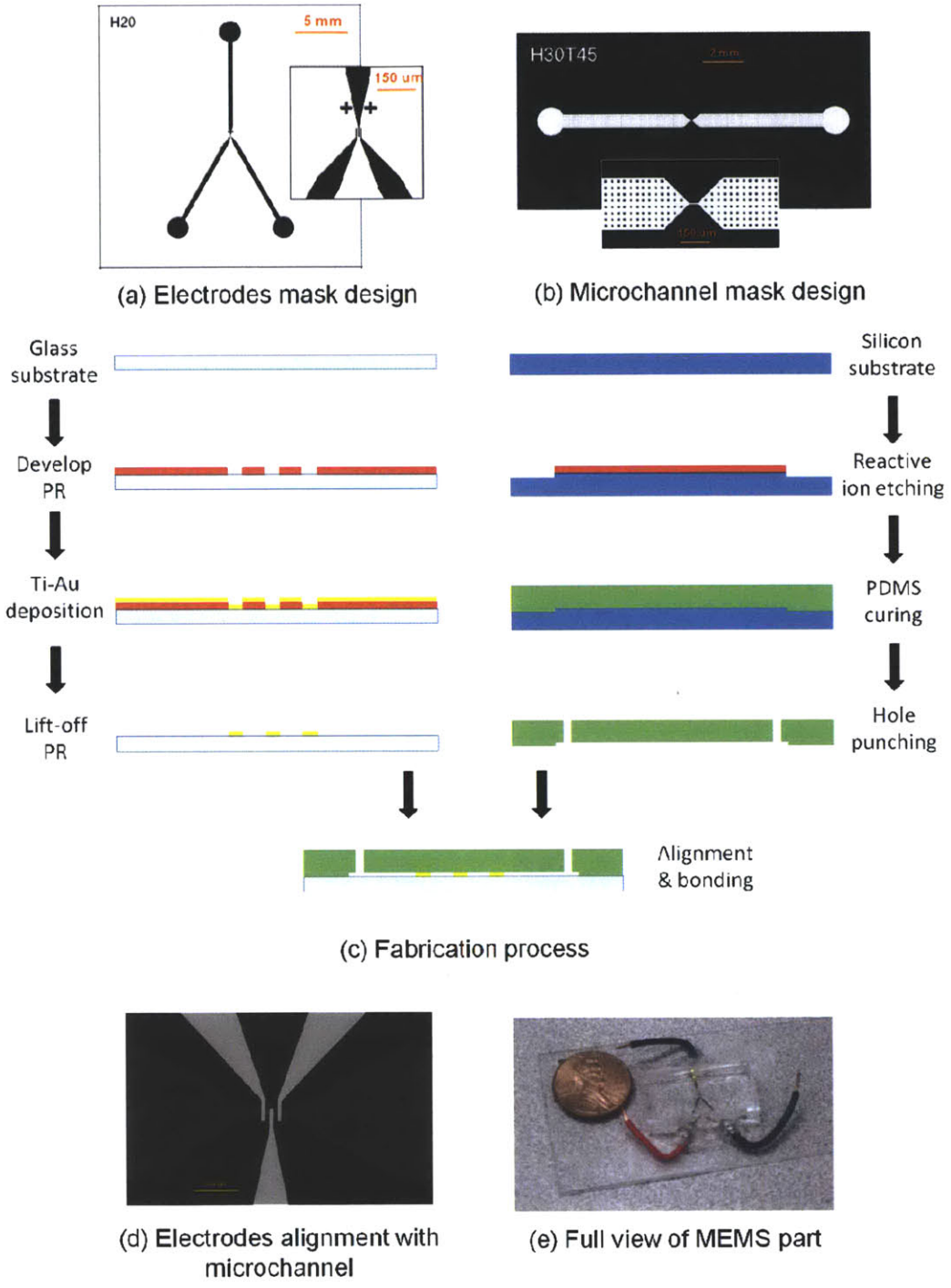

Figure 12. Illustration of MEMS fabrication: (a) mask design of 1" by 1" glass substrate with electrodes (left) and center zoom-in (right), (b) mask design of 1" by 0.5" silicon mold for microfluidic channel (top) and center zoom-in (bottom), (c) illustration of overall fabrication process, (d) microscopic view of the channel and (e) full view of the microfluidic device.

Firstly, electrode parts are fabricated on 0.500mm-thick 6-inch Pyrex glass wafer (Sensor Prep Service Inc.) Wafers are dehydrated on hot plate at 115°C for 3 minutes to get rid of moisture that degrades resolution of photo resist (PR). Wafers then spin coated with a negative PR, NR71-3000P (Futurrex Inc.), at 3000 rpm for 40 seconds. 3-mininute prebake at 140°C is followed by 10-second UV (365nm) exposure. After 3.5-minute post exposure bake at 110°C, wafers are developed for 25 seconds in RD6 developer solution. Then, wafers are washed by DI water and dried with nitrogen gas. Next, 10-nm titanium adhesion layer and 100nm gold electrode layer are deposited on the wafers. Lift-off process follows. A 6-inch wafer makes 16 electrode parts of the microfluidic device.

6-inch silicon wafer is used to make the master mold for the microfluidic channel. After developing PR, AZ5214 (Clariant Corp.),wafers are etched in depth of 5μm by reactive ion etching (RIE). PR is stripped out after RIE, and then the silicon mold is ready. The microfluidic channel is fabricated of polymers called Polydimethylsiloxane (PDMS) on a silicon mold. PDMS is widely preferred and used material in microfluidic fabrication in terms of its transparency, low cost, biocompatibility and ease of fabrication. First PDMS base gel is mixed with PDMS curing agent in ratio of 10:1. After de-gassed in a vacuum chamber for 1 hour, PDMS mixture is poured on the silicon mold whose surface is coated by trichlorosilane ($HSiCl_3$) to prevent adhesion to silicon surface. Baked on hot plate at 95°C for 2 hours, PDMS is solidified. Peeling off PDMS and cutting by each 1-inch-by half inch cell, 32 microfluidic channel parts are ready for the next step and the silicon mold is reusable to produce more PDMS cells.

After fabrication of electrodes and PDMS cells, oxygen plasma is used to bond both fabricated electrodes and microfluidic channel. After plasma excitation of the surfaces, two parts are aligned and bonded within a minute under microscopic observation. Two hours of heat treatment afterwards results in strong covalent bonding between PDMS and glass substrate. After bonding two substrates, gold pads at the end of electrodes are soldered with AWG-22 copper wires and ready for the connection to impedance converter circuit.

3.3. Circuit Board Design

A printed circuit board is designed to perform EIS. The board consists of a commercial integrated circuit (IC) chip, passive components and other peripherals for connections to power source and FPGA module. The commercial chip is impedance to digital converter over the frequency range up to 100 kHz. FPGA board plays a role of a bridge of instructions and data between PC and the impedance converter. Overall block diagram of electronic part of EIS-based malaria diagnostic system is shown in Figure 13. The user inputs parameters and commands for EIS at PC side, the data are transferred to FPGA via USB. Because the USB controller utilizes virtual I/O ports, the user can assume that there are a number parallel links for inward and outward data transfer. FPGA runs a finite state machine that interprets the data from PC and control an I^2C master module to communicate with the impedance converter chip. Parameters settings and commands are sent to the impedance converter chip after several cycles of

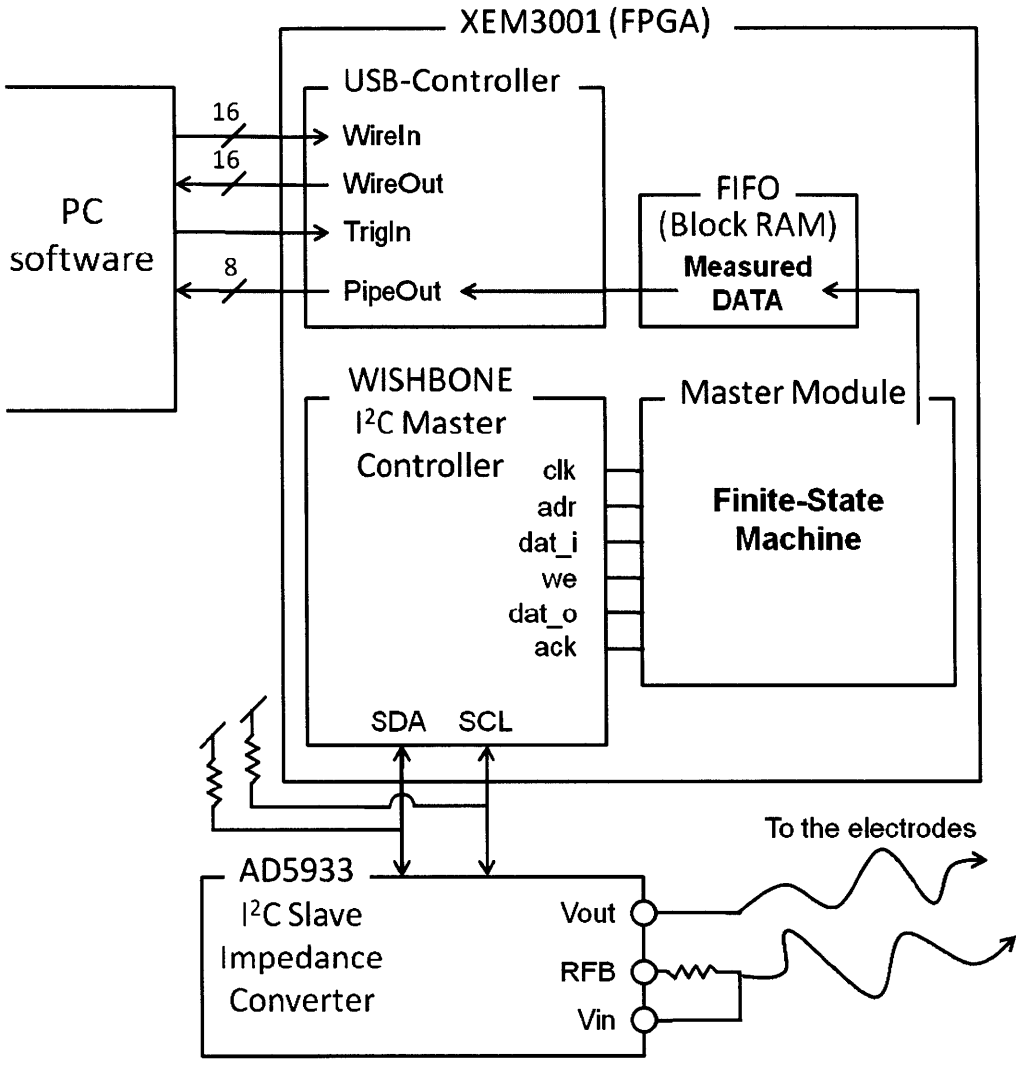

Figure 13. Overall block diagram of electronic part of the system.

bidirectional communication. At given settings, the impedance of the device under test connected to the probes is measured, and the result is sent back to FPGA. FPGA collects the data and send them to PC via USB again.

3.3.1. Description of the Function

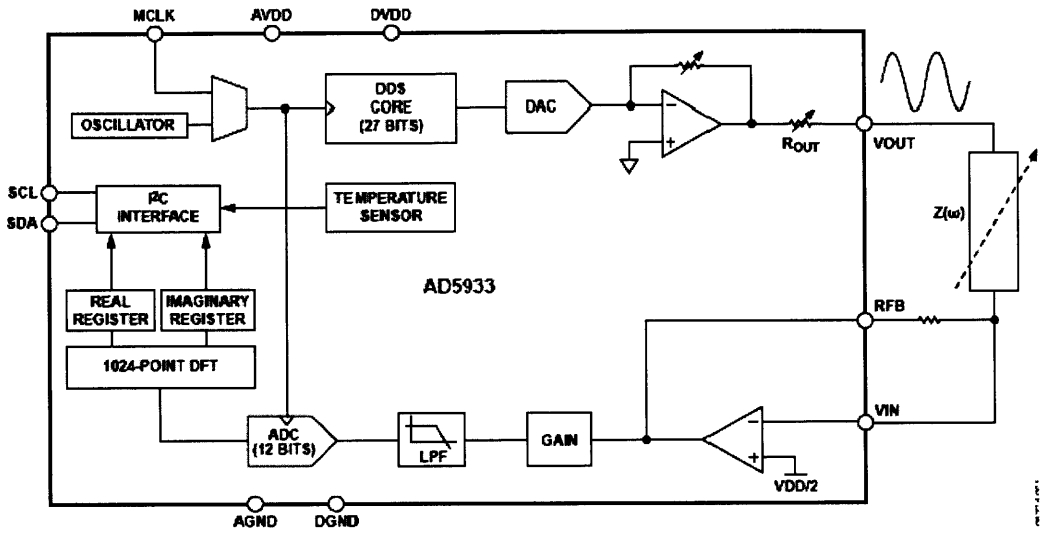

Figure 14. Functional block diagram of AD5933 [15]

Electric impedance is measured by a 1 MSPS, 12-bit impedance converter chip, AD5933 (Analog Devices Inc.), and its functional block diagram is shown in Figure 14. Sinusoidal excitation signal is applied to one of a pair of electrodes in the microfluidic device. Circuit board reads the resulting current and calculates discrete Fourier transform (DFT) of it. Since DFT measures energy of signal at a frequency, impedance at certain frequency can be obtained as following equations.

The DFT of a sequence of N complex numbers $x_0, \ldots, x_{N-1}$ is given by:

$$X_k = \sum_{n=0}^{N-1} x_n e^{-j\frac{2\pi}{N}kn} = R + j\,I$$

$$A_k = |X_k| = \sqrt{R^2 + I^2}$$

$$\varphi_k = tan^{-1}\left(I/_R\right)$$

The magnitude and phase of impedance Z is obtained by following equations:

$$Z = \frac{v_I}{i_O} = \left|\frac{V_I}{I_O}\right| \angle \varphi_I - \varphi_O$$

$$= \left|\frac{V_I R_{fb} R_A}{V_O}\right| \angle - \varphi_O$$

$$= \frac{Gain\,Factor}{\sqrt{R^2 + I^2}} \angle - tan^{-1}\left({}^{I}/_{R}\right)$$

where v_I, i_O, V_I, I_O, φ_I, φ_O, R_{fb}, R_A, V_O are sinusoidal input voltage, output current, input voltage magnitude, output current magnitude, phase of input signal, phase of output signal, feedback resistance, internal amplifier gain, output voltage magnitude, respectively. The impedance converter chip stores the real (R) and imaginary (I) codes of DFT at two 16-bit registers. The two data registers can be accessed by FPGA or a user via I2C protocol.

In practice, the gain factor and the system phase offset are calibrated first by measuring a resistor of known impedance. With the calibrated parameters, unknown impedance can be measured. The gain factor and the system phase offset may change at different frequencies, so calibration is required at each frequency of interest to obtain accurate data.

3.3.2. Printed Circuit Board Design

Once the circuitry is confirmed to work in a prototype board, a two-layer PCB size of 2" by 1.5" shown in Figure 15 is designed to ease electrical connection between hardware. Electrodes at microfluidic device are connected to VOUT and VIN ports of AD5933 through RG-316/U coaxial cable and SMA connector on the PCB. A 20-pin connector is placed at the side of PCB for connections to power lines and I2C clock and data lines of FPGA board. Feedback resister bank can select a proper resistor or combination of resistors according to the target impedance. With this bank, adjustment of feedback resistor is much easier at PCB. For analog supply voltage of AD5933 (AVDD), external voltage source can be supplied via a BNC connector. The PCB has option to use the external power source or 3.3V supply from XEM3001v2 FPGA board.

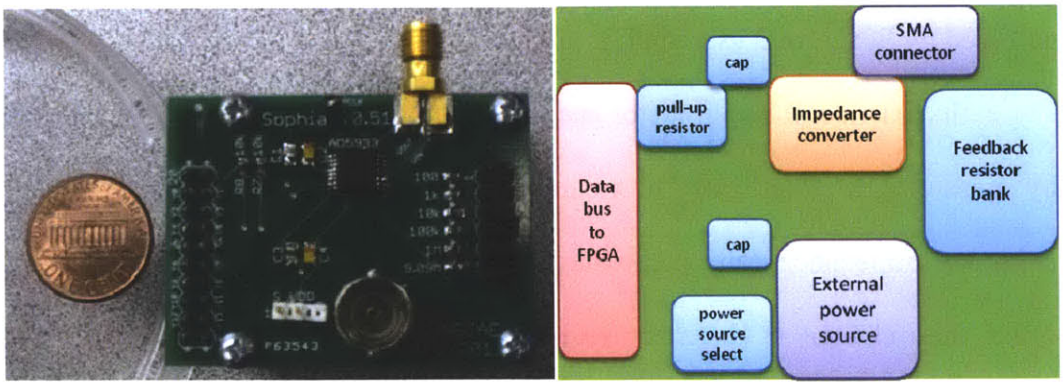

Figure 15. A 2" by 1.5" printed circuit board (PCB) for impedance converter.

3.3.3. FPGA Programming

An Opal Kelly XEM3001v2 board featuring Xilinx Spartan FPGA connects the impedance converter circuit board and user interface software. It decodes commands from the user interface (UI), controls the impedance converter, receives data from AD5933 chip, and sends them back to the user. Verilog hardware description language (HDL) is used to program those functions.

Communication between FPGA and UI is carried out via USB cable. XEM3001v2 has a USB controller module, and Verilog codes for instructions and data transfer are supported by its own library called FrontPanel [16]. Using the library, UI transfers instructions and configuration data to the master module in FPGA.

Communication to AD5933 is trickier compared to UI side. AD5933 only supports I^2C serial bus interface. I^2C is a two-wire interface able to connect multiple masters and slaves using one data line (SDA) and another clock line (SCL). To ease the job of being compliant to the protocol, a sub-module (WISHBONE in Figure 13) is integrated in FPGA. The master module in FPGA controls AD5933 chip and retrieves impedance data from it through the sub-module.

Contrary to instructions and configuration data, the impedance data from continuous measurements take up a large volume. 4-byte impedance data point can be stacked in rate of up to 4 kB/s. Therefore, data transfer should be carried on in speed of 4 kB/s or above. While general purpose data transfer functions,

WireIn and WireOut, ars slow (up to 1.6 kB/s), the block data transfer function, PipeOut, has higher data transfer rate ranging from 100 kB/s for small data block size and up to 38 MB/s for lager block size [17]. Bulk data transfer reduces overhead such as several layers of setup including those at the firmware level, API level, and operating system level, required at each data transfer. To do bulk transfer of impedance data, a FIFO is added using built-in block RAM of Spartan 3 FPGA.

Another function is necessary in FPGA because of the slow data rate of WireIn and WireOut. During continuous measurements, the impedance converter is repeatedly triggered and sending data to FPGA. If the repeating trigger command is called by the UI, it degrades the speed of overall system due to the bottleneck of the data transfer rate. Therefore, this function is implemented in the FPGA. Master module is programmed to trigger AD5933, retrieve data, and repeat for the given number of times from UI, so that overall system throughput is determined by the performance of AD5933.

3.4. User Interface Software

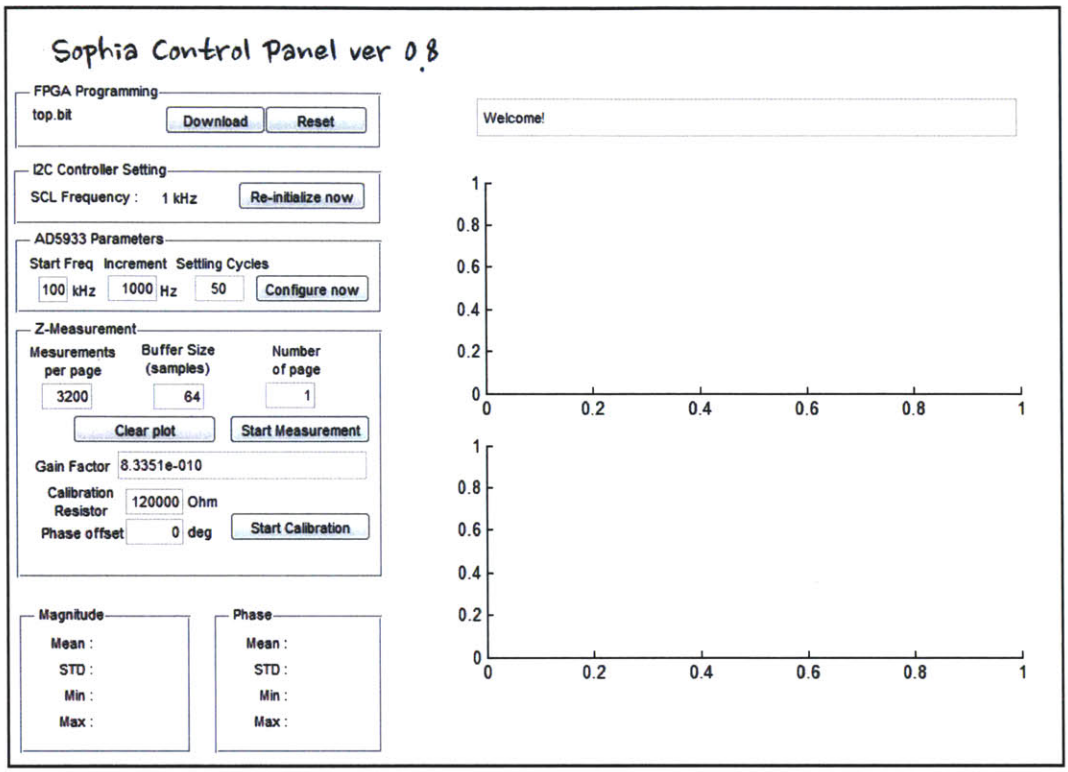

Figure 16. User interface for impedance measurement

A custom MATLAB GUI program shown in Figure 16 is built for user interface. The GUI does jobs listed below:

- Download Verilog codes to FPGA.
- Set clock frequency for I2C protocol and initialize master module.
- Set parameters of impedance converter such as excitation signal frequency, frequency increment in frequency sweep function and number of settling cycle in ADC.

- Command FPGA to conduct continuous measurement for given number of measurement and send bulk data in given buffer size.
- Calculate and plot magnitude and phase, and show statistics.
- Calibrate the gain factor and the system phase with resistor measurement.
- Save the received data in MATLAB workspace for post-process.

3.5. Sample Preparation

Human blood samples were prepared with and without the malaria parasites at Nanomechanics Laboratory (MIT, Cambridge, MA). Plasmodium falciparum parasites were cultured in leukocyte-free human RBCs (Research Blood Components, Brighton, MA) under an atmosphere of 5% O2, 5% CO2 and 95% N2. The blood samples were cultured at 5% haematocrit in RPMI culture medium 1640 (Gibco Life Technologies, Rockville, MD) supplemented with 25 mM HEPES (Sigma), 200 mM Hypoxanthine (Sigma,St. Louis, MO), 0.20% NaHCO3 (Sigma, St. Louis, MO) and 0.25% Albumax I (Gibco Life Technologies,Rockville, MD). Parasite cultures were routinely synchronized in ring stage by using Sorbitol lysis 2 h after merozoite invasion and a Midi MACS LS magnetic column (Miltenyi Biotech, Auburn, CA). Parasites and RBCs are cultured in body temperature (37 °C) then cooled down to room temperature (20 °C) before every experiment. As human RBCs stay in a very narrow pH range from 7.35 to 7.45, a buffer solution, phosphate buffered saline (PBS), was used to maintain pH of blood at around 7.4. The osmolarity and ion concentration of the

buffer solution matches those of the human body (isotonic) [23], so blood samples were diluted with PBS.

In addition to red blood cells, polystyrene microspheres (Phosphorex, Inc., Fall River, MA) are prepared. Theses microspheres have variety in their size, color, and surface function coating. To simulate blood sample, PBS with the same concentration was used to buffer the microsphere solution and dilute it. Before each use, the microspheres were sonicated to avoid cluster of microspheres.

Chapter 4

Results

4.1. Preliminary results

Before the overall system tested blood sample for malaria, preliminary experiments below were conducted at MicroNanofluidic BioMEMS laboratory (MIT) to verify that each part of the system worked correctly and that the concept of EIS-based malaria infected cell detection is feasible. In all of these EIS experiments, the microfluidic channel and particle flows were monitored at an inverted microscope (IX-71, Olympus), and were recorded by the attached CCD camera (SensiCam, Cooke Corp). Live observation and video using Image Pro Plus 5.0 (Media Cyberneteics Inc.) were used to correlate target cells or beads to their EIS data. The blood samples and microsphere solutions were fed into the microfluidic device from a syringe pump (PHD 2200, Harvard Apparatus) through a tube. Figure 17 shows the setup of the microscope, the syringe pump, and the electric probe connection.

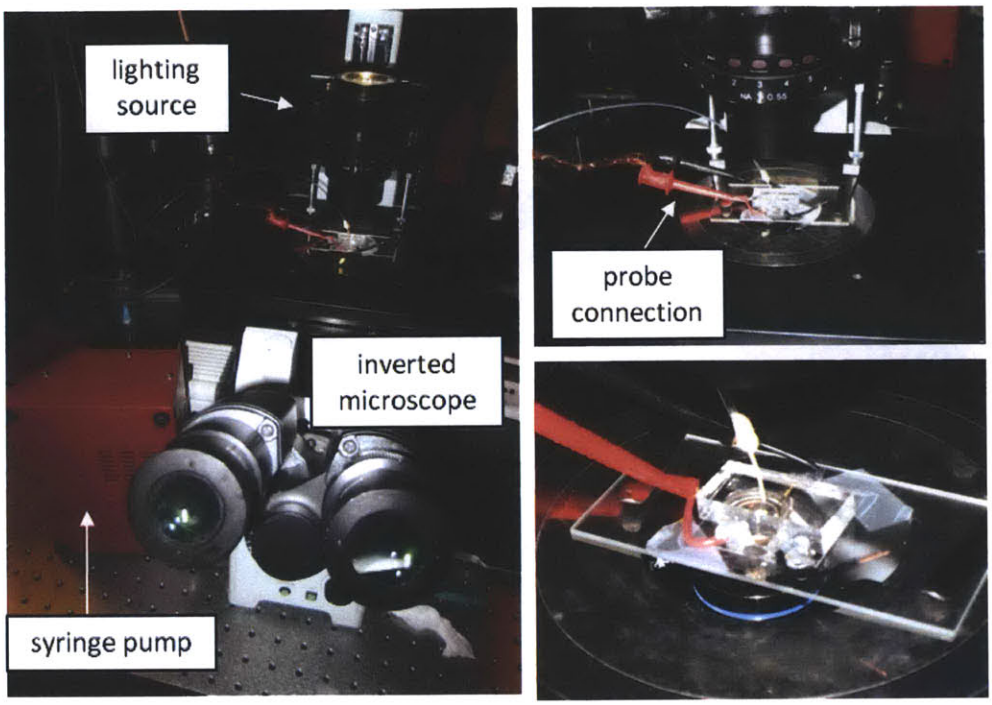

Figure 17. Experiment setup: the syringe pump is located next to the microscope (left); one of lightings system of the inverted microscope shines from the top (top right); tube is connected to inlet, and mini-grabber style probes are connected to the electrodes of the microfluidic device (bottom right).

4.1.1. RBC Counting with Impedance Measure Equipment

An experiment with impedance measurement equipment was conducted to verify that the fabricated microchannel and electrodes were working as designed. Electric impedance spectroscopy on a healthy human blood sample (uninfected RBC) was performed with 4980A LCR meter (Agilent Technology, Inc.) over a frequency range from 100 kHz to 1 MHz. The LCR meter was connected to PC via GPIB protocol, and fully controlled by a custom LabVIEW (National Instruments, Inc.) program. With a pair of electrodes, it was possible for the

experiment setup to measure continuously the electric impedance of the microfluidic channel of MEMS device with or without RBC.

Showing 35.8 dB signal-to-noise ratio (SNR) in terms of the ratio of RBC signal and noise in reference signal, it could measure the number of RBCs passing from the collected impedance data (Figure 18). From the experiment, the design of the microfluidic channel and the electrodes was confirmed to work for EIS. Starting from 50x diluted blood and up to 4x diluted blood, RBCs flowed without clogging in the micro channel. Higher concentration was not tested since the spacing between each cell was too close and the analysis on single cells was inaccurate. Another important aspect is the throughput of the system. The maximum output data rate of continual measurement by the LCR meter was 19.4 Hz, which is limited by the GPIB protocol. In practice, the system could detect up to only around 100 cells per minute because of non-uniform spatial distribution of the cells.

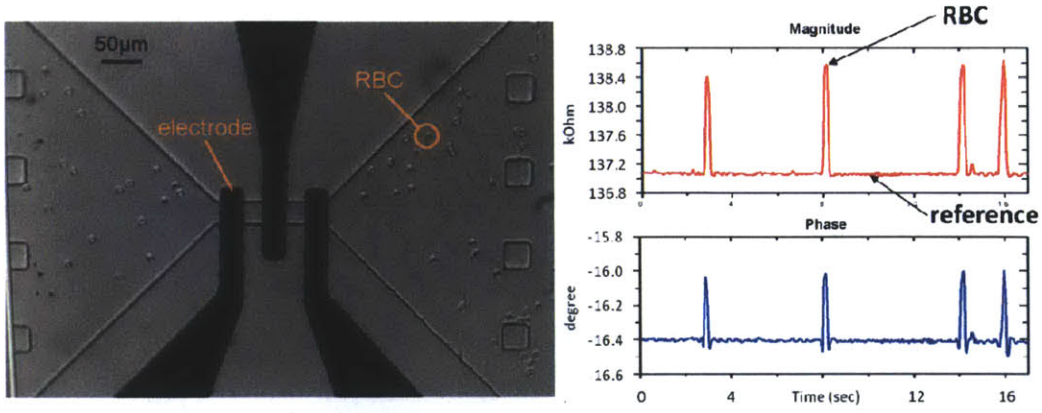

Figure 18. RBC counting experiment with LCR meter

4.1.2. EIS with Printed Circuit Board and Shielded Probes

A similar experiment to 4.1.1 was performed using the printed circuit board described in 3.3. Instead of human RBCs, 5.1μm-diameter (σ = 0.4μm) polystyrene microspheres whose volume is similar to human RBC were used in the measurement. The reason of using non-bio beads is to characterize effects of surface charge of particles in the following experiment.

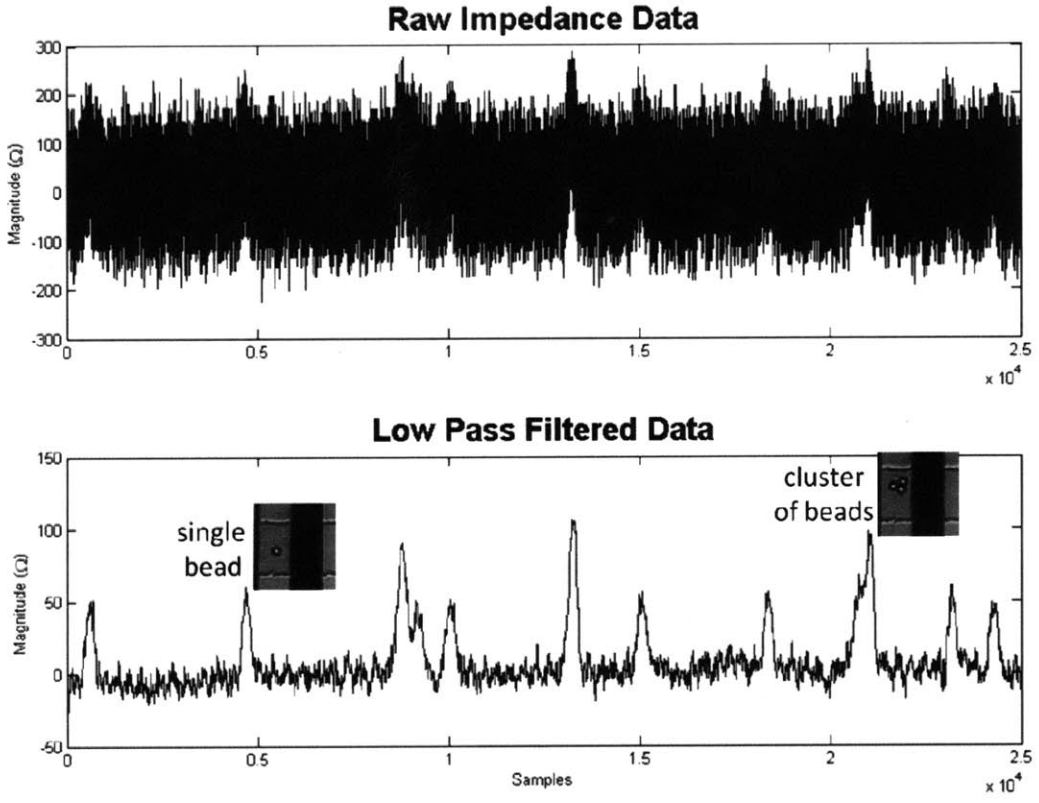

Figure 19. Plain polystyrene beads counting with impedance converter PCB in unshielded two-terminal configuration

Figure 19 shows the raw impedance data of plain micro-bead and filtered data measured by the circuit board in unshielded two-terminal configuration. The

impedance measurement result seemed very noisy, and sensitivity of the printed circuit board was very low compared to that of the LCR meter. After applying a FIR low pass filter to suppress noise in high frequency, SNR (in terms of the ratio of bead signal to noise in the reference) of single bead was only 20.0 dB and lager of a cluster of multiple beads. Despite low SNR, the result first showed particle volume dependency of impedance. Second, the result promises that a PCB can replace bulky electrical equipment, so that entire EIS system can be miniaturized in a small board or even in a chip. Third, the PCB enhanced data rate of the impedance measurement from 19.4 Hz to 500 Hz. The increased speed of impedance measurement can lead to a high throughput EIS device for biological cells unless it is resulted from the sacrifice of SNR.

However, the sensitivity of EIS by PCB could be significantly improved in shielded two-terminal configuration. The reason of low sensitivity at the first measurement was the stray capacitance between two probe lines, and the problem was solved by shielding those lines. As depicted in Figure 20, stray capacitance introduces bypass path of current. The ADC at the end of the VIN port reads consequently the sum of the current through the device under test (DUT) and the bypass current, resulting the sensitivity of admittance ($\Delta Y/Y_{DUT}$) to be degraded by a factor of $\frac{Y_{DUT}}{(Y_{DUT}+Y_{stray})}$.

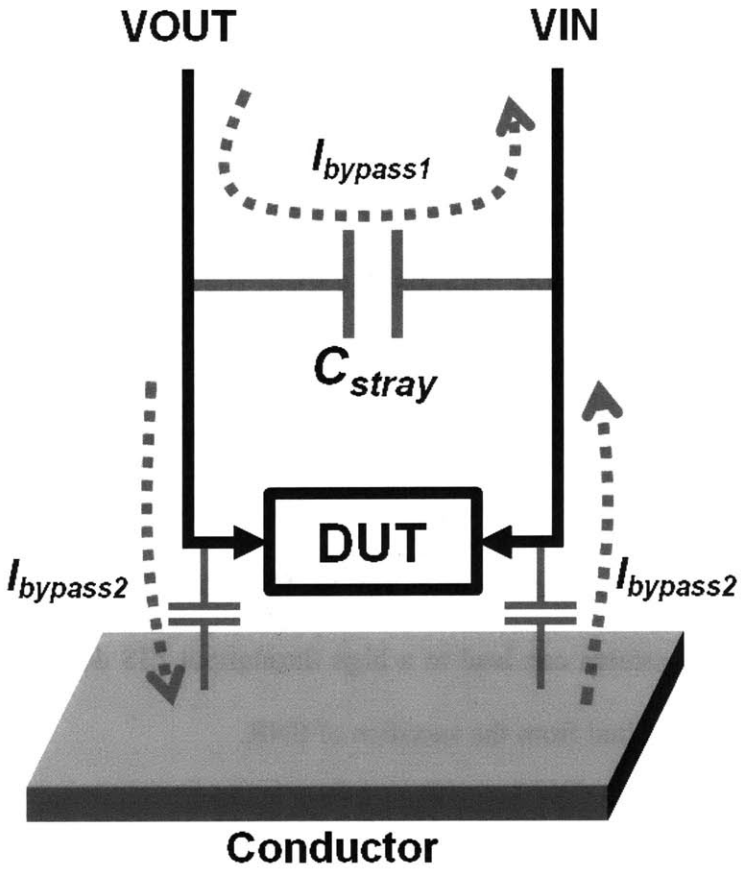

Figure 20. Stray capacitance between two probe lines

To eliminate the stray capacitance and interference by conductor near DUT, such as microscope or human body, the circuit board was modified to shielded two-terminal configuration [25] as shown in Figure 21. By putting grounded shields on the probe lines, stray capacitance can be minimized. The EIS measurement on the 5μm micro-beads showed that SNR, in terms of bead signal and reference noise, was improved by ~15.0 dB. Thus, the circuit board could be used in the following experiments.

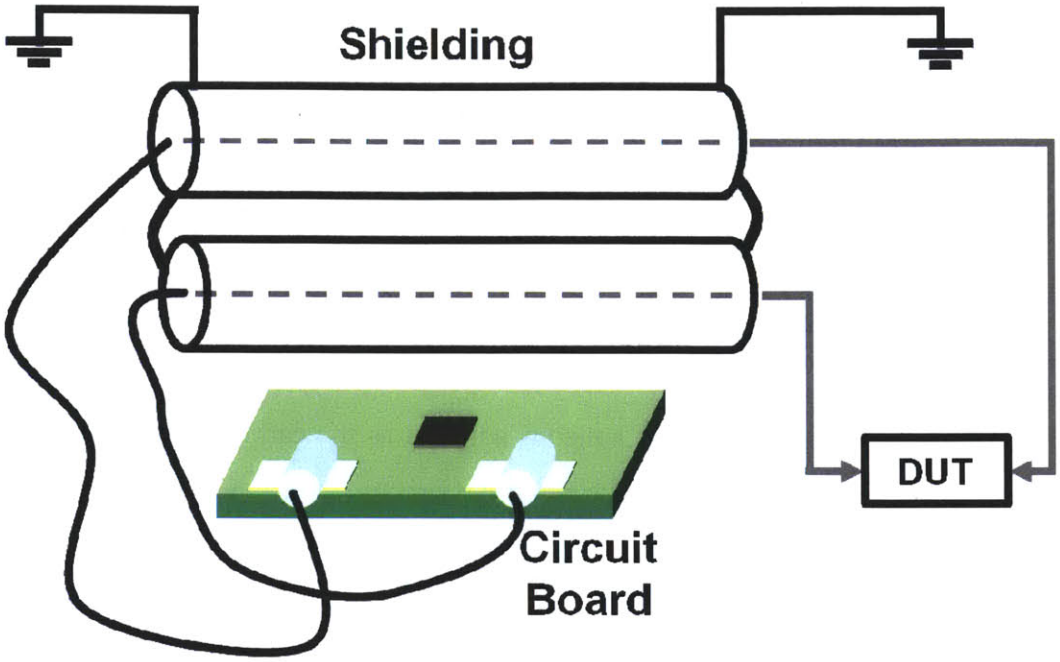

Figure 21. Shielded two-terminal impedance measurement configuration

Estimated from the impedance measurement of a resistor, the noise of the impedance converter board was as low as 0.1% (-60dB). The source of the noise is the DDS of the AD5933 impedance converter chip. The SNR of the excitation signal of the chip, the ratio of the root-mean-square (rms) value of the measured output signal to the rms sum of all other spectral components below the Nyquist frequency, is 60dB [15]. During the impedance measurement, -60dB noise in the sinusoidal excitation signal induces -60dB noise in the current over the DUT. The noise is collected by 12-bit (72dB) ADC, and DFT is calculated from the ADC outputs. Thus, the SNR of the circuit board is limited to 60dB.

4.1.3. Micro-beads Differentiation

Before the investigation of blood cell with and without malaria parasites, the effect of surface charge of particle on EIS was studied. Two types of microspheres (beads), plain one without any surface function and another coated to have carboxyl (-COOH) surface function, are prepared. COOH-coated beads have negative surface charge in aqueous solution as the carboxyl function loses proton (H^+) by water molecules and remains attached to the bead with negative charge. Figure 22a illustrates two microspheres. Since the size of two is same, they cannot be visually differentiated by size and one has to be dyed. Thus, COOH-coated beads are made to be fluorescent for visual differentiation to plain ones. The fluorescent beads absorb 460nm blue light and emits 500nm green light. Figure 22b depicts that fluorescent beads are distinguishable from the other plain beads though they are similar in their size.

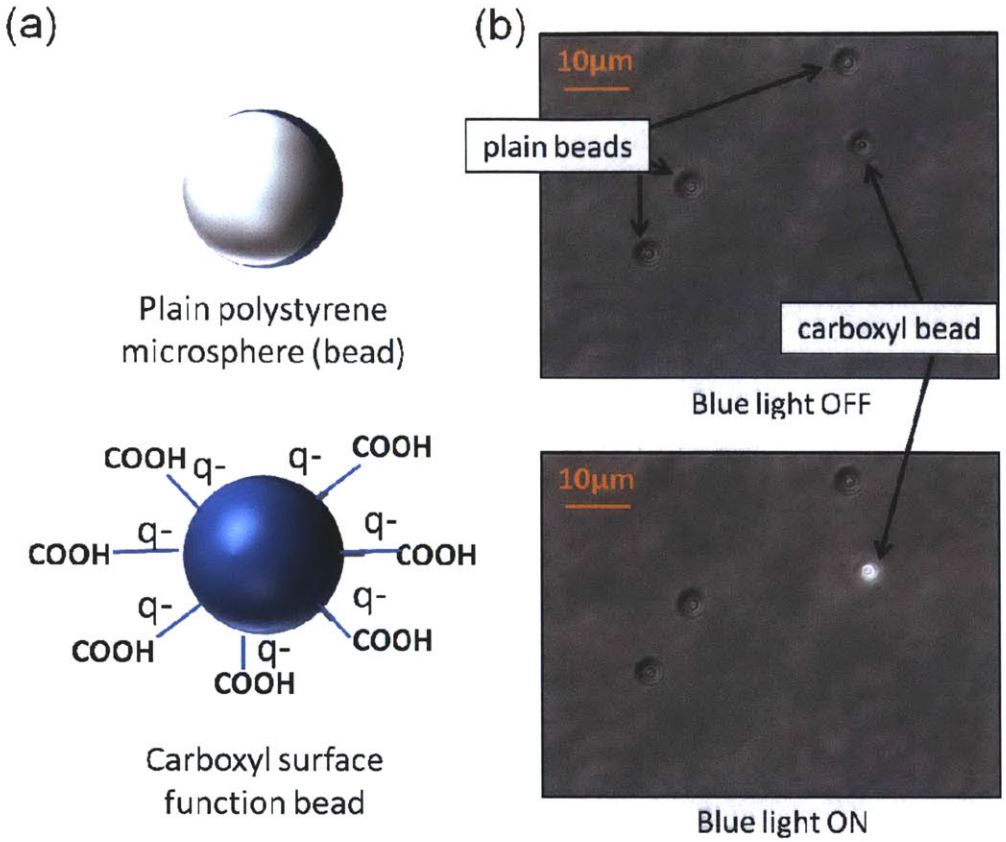

Figure 22. Illustration (a, left) and differentiation of micro-beads (b, right)

The size of the beads is chosen to imitate the volume and flow dynamics of RBC. Two types of beads have nominally 5μm diameter, but there were variations in their size. The plain micro-beads have mean diameter of 5.1μm with standard deviation of 0.4μm. The carboxyl beads have mean diameter of 4.6μm with standard deviation of 0.4μm, ~10% smaller in mean diameter. The effect of their size difference on electric impedance was taken into account in data analysis afterwards.

Figure 23 shows snapshots of an EIS measurement on plain and carboxyl beads. The carboxyl beads are emitting fluorescent light so distinguishable from dark plain beads.

(a) t = 14s

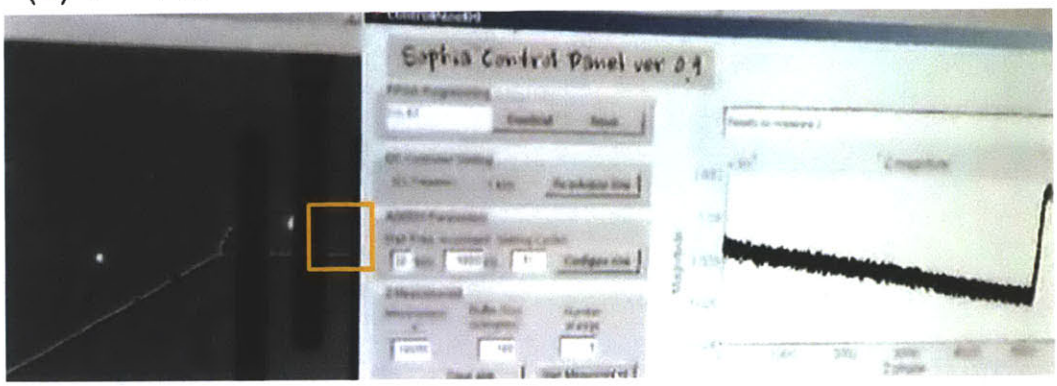

(b) t = 18s

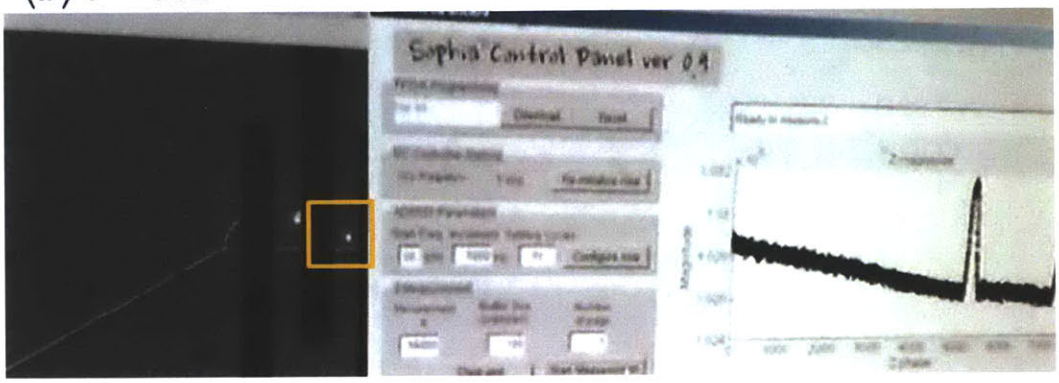

(c) t = 28s

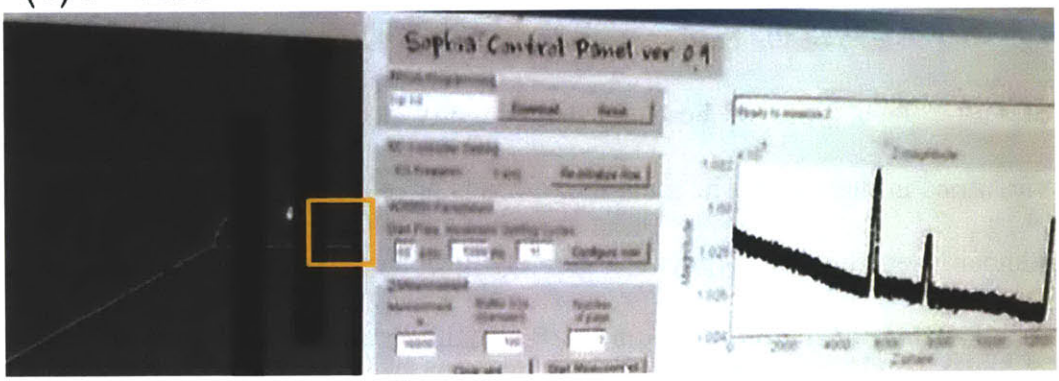

Figure 23. Real-time monitoring of micro-beads in the microfluidic channel and their impedance spectroscopy: plain (dark) and carboxyl (bright) beads.

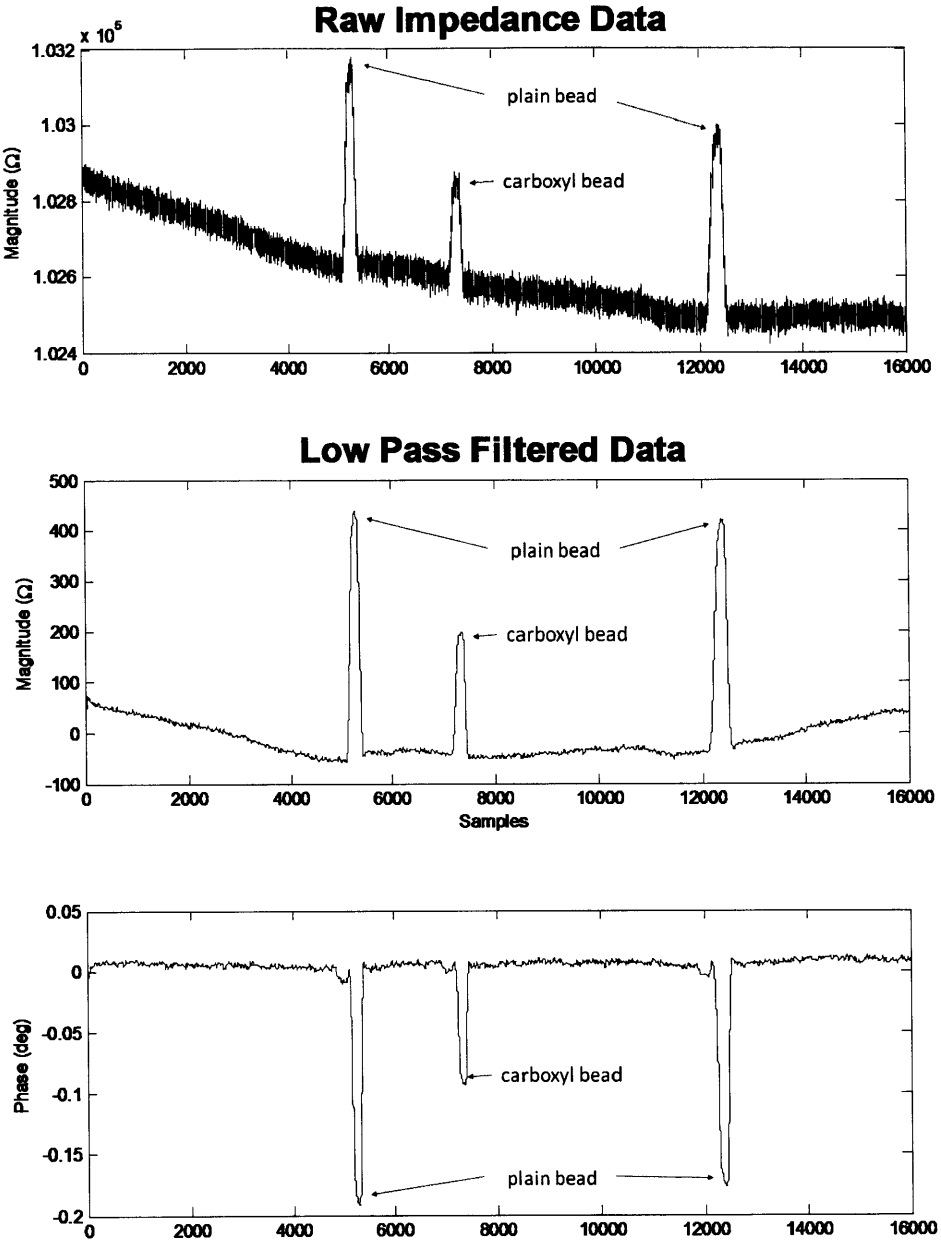

Figure 24. Electric impedance spectroscopy on two types of microspheres: the large peaks are plain beads and the small peak is a carboxyl bead.

Comparing the resulted peaks in Figure 24, both magnitude and phase have significant difference in two types of beads. Plain beads made larger change

in impedance than carboxyl beads at the tests in two microfluidic devices. Figure 25 and Table 3 summarize the experiment data, showing the ratio of mean magnitude peak values to be 185% and 170% at each device and of mean phase peak values to be 2.

Before jumping into the conclusion that the carboxyl surface function lowered the impedance of beads, the difference in the sizes of beads has to be considered here. Knowing that polystyrene beads are highly resistive ($\sigma = 10^{-16}\,\mathrm{S/m}$) and PBS solution is rather conductive ($\sigma = 1.2\,\mathrm{S/m}$), the microchannel can be modeled as a conducting cylinder with an insulating sphere inserted in it. Then, the Maxwell's approximation equation can be applied to the

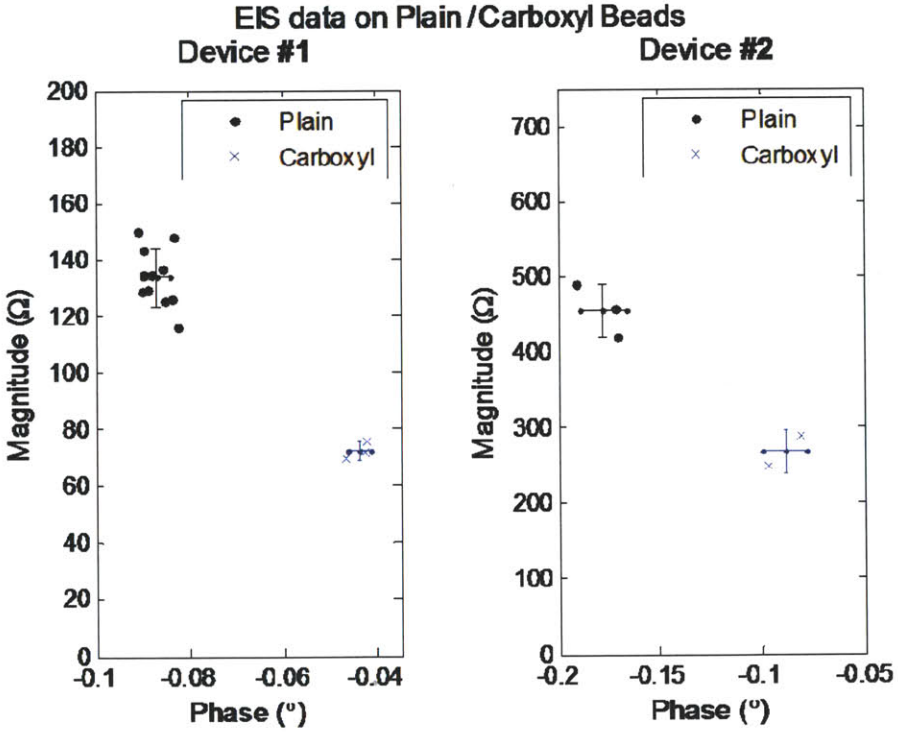

Figure 25. Summary of EIS on micro-beads

Table 3. Summary of EIS on micro-beads

Device		#1		#2	
		Magnitude (Ω)	Phase (°)	Magnitude (Ω)	Phase (°)
Plain	Mean (A)	133.73	- 0.0870	455.17	- 0.1778
	STD	10.30	0.0030	34.86	0.0114
Carboxyl	Mean (B)	72.118	-0.0437	267.27	-0.0890
	STD	3.026	0.0023	28.87	0.0108
Ratio	A/B (%)	185.43%	199.08%	170.30%	199.78%

model, and the increase in impedance of the channel is proportional to the volume fraction of the micro-beads [24]. The ratio of the volume fraction of two beads is only 1.324 which is 0.520 and 0.379 less than the ratio of magnitude means at each device, respectively. Therefore, the difference of peak heights is also resulted from the surface charge of carboxyl coated beads which makes the beads more conductive. In conclusion, EIS with the circuit board in shielded two-terminal configuration could differentiate two groups of micro-spheres.

Though the groups of beads with different surface charge could be differentiated in a device, the same beads resulted in different impedance values at another device. The reason for the difference was the device dimensions which varied in each device due to the process variation in photolithography, silicon etching, PDMS fabrication, and wiring. The width of the electrodes and channel were different. Some parts were more etched and others less, thus the depth of channel was different for each device. Alignment and fluid access hole were made by hand, and those also caused the difference. In addition to the device variation, the ion concentration variation of the sample affected the impedance as well.

4.2. *P. Falciparum*-Infected RBC Detection

Human blood with ~1% malaria parasitemia was tested. This experiment used an inverted microscope equipped with both a 40x lens and a 2.5x magnifier at Nanomechanics Laboratory (MIT) to achieve enough resolution to visualize the parasites inside of RBC. 10x diluted blood sample was fed into the microfluidic device. The flow rate was accurately limited to 5nl/min or less to make the cell flow recordable. The circuit board in shielded two-terminal configuration

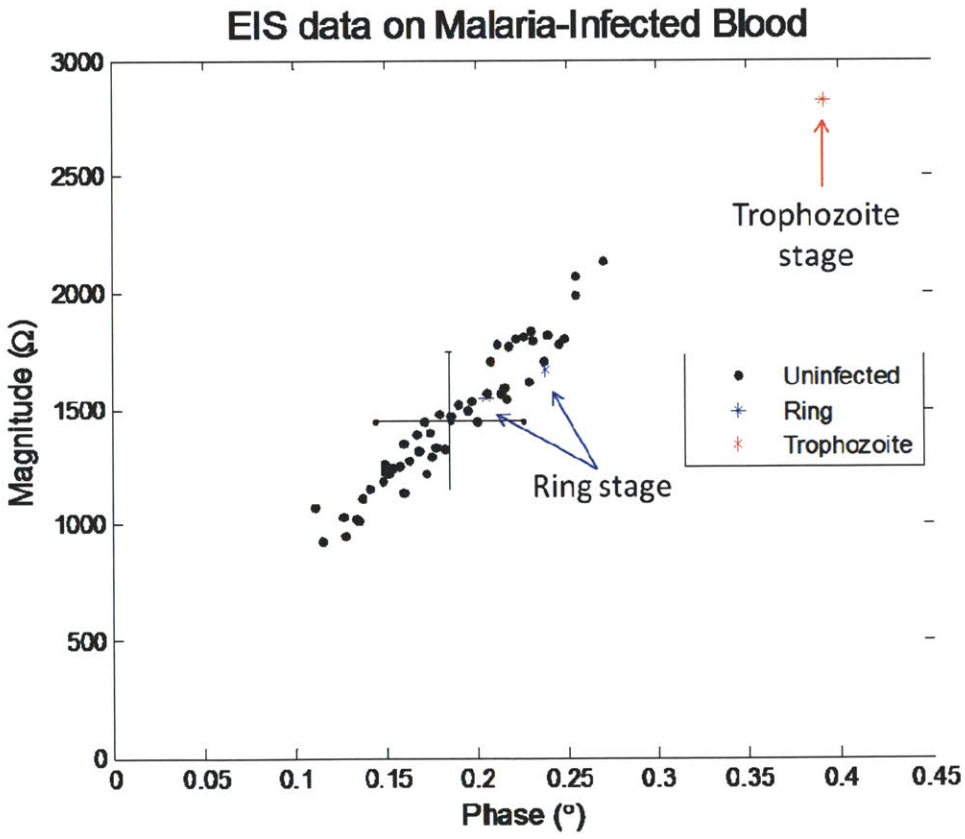

Figure 26. Scatter plot of EIS data of RBCs (n=55): three of them were invaded by *P. falciparum* parasites. Among three, two were at ring stage (blue) and the other is at trophozoite stage (red).

measured the electric impedance of flowing cells.

EIS data of 55 RBCs are presented in Figure 26. Because the blood sample was in the early stage of malaria, the portion of infected cell data was small. Among 55 measured cells, three cases were confirmed as malaria-infected cells by visual inspection. Before passing through the channel and over the probe electrode, the cells were inspected by 100x magnification as shown in Figure 27. Two of the infected cells were in their ring stage, the very early stage of malaria parasite infection, and the other one was in its early trophozoite stage, the following stage after the ring stage.

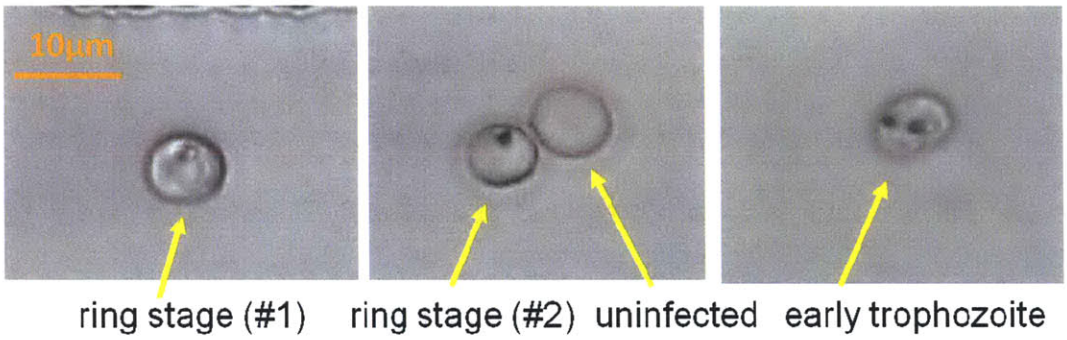

Figure 27. Visual inspection of three malaria infected RBCs

The scatter plot shows a cluster and an isolated point of EIS data. The cluster contains EIS data of uninfected RBCs and ring stage RBCs, and the isolated point is the trophozoite stage RBC. While uninfected RBCs and ring stage RBC are indistinguishable from the scatter plot of their EIS data, EIS data of the trophozoite RBC appeared separate at high magnitude and phase region in the plot.

Chapter 5

Conclusions

This chapter concludes this master degree study on malaria-diagnostic system based on electric impedance spectroscopy.

5.1. Miniaturized Microfluidic EIS System

First of all, a small-sized circuit board to conduct continual impedance measurement in the speed of 500 Hz is built. Combined with the fabricated microfluidic device, the EIS system could count red blood cells or tiny particles ($D < 10\mu m$) flowing in the microfluidic channel. The system could also see the effect of surface charge of the micro-sized particles on the electric impedance, promising the sorting ability of various particles and biological cells.

The speed of the electrical probing is a great merit of EIS. It easily exceeds the limit of ordinary video recording speed, so that the electronic probe sensed the fast particles while the video missed them in the experiments (data not shown). Therefore, it can get rid of the necessity of high-speed video camera in

high throughput optical probing system, and EIS can provide new observing methods for high-throughput microfluidic system.

The frequency range of the circuit board is limited by the spec of the commercial impedance converter whose maximum is 100 kHz. Because of the cell membrane capacitance, higher frequency is required to probe intracellular properties. Thus, this study more focused to investigate cell membrane properties such as surface charge.

5.2. Malaria Diagnosis

As reported by [8], malaria parasites perturb the ion composition of its host cell affecting host cell's membrane, and the impedance change was measurable after invasion at the low frequency range below 50 kHz. From the motivation that the proposed EIS system would probe the electrical properties of RBC membrane in flowing condition, malaria-infected blood sample in its early stage was tested.

The EIS result of malaria-infected blood is well summarized in Figure 26, and it was a preliminary measurement in detection of *P. falciparum*-infected RBC at a microfluidic device. Comparison to the bead experiment concludes that the surface charge of RBC was significantly different between two groups, one group of uninfected and ring stage RBCs and another group of the trophozoite stage RBC. Though there were only few data of infected cells, the experiment result can be explained in the sense that the malaria parasites in the ring stage had not changed or made little change yet of host cell membrane, so the membrane

property was similar to other healthy uninfected RBCs, and in the sense that the parasite grew in the host cell (trophozoite stage), so it perturbed the membrane property in measureable degree.

Following the preliminary measurement, more analysis is needed to understand malarial effect on electric impedance of RBC and to develop a rapid diagnostic tool based on EIS. The trend for the later stage malaria-infected RBCs has to be investigated to accurately model malarial impedance change: whether other trophozoite stage cells express the similar impedance, whether malaria causes monotonic increment of impedance, and whether the schizont stage cells can be differentiated from the other stage cells. More importantly, EIS at high frequency needs to be studied to see if it can probe intracellular modification or the malaria parasite, for detection of ring stage malaria which is important for early diagnosis.

To pursue label-free detection of malaria-infected RBC, verification of correlation between cell type and impedance data fully relied on visual inspection. Some difficulties have come up from that condition. First, the flow rate of RBCs has to be slow enough for visual inspection while or before they pass through. When the flow rate came down as low as 5nl/min, it is very difficult to control the flow by pump. Slow flow rate introduces the second difficulty. As time goes, water evaporates from PBS solution and it causes RBCs to squeeze by osmosis. Therefore, the maximum experiment time is limited unless adding water in during the measurement. Also, the EIS measurement always has to run simultaneously with live observation of RBCs. These difficulties should be considered in the

following studies. Once the correlation is proved, EIS can be conducted in high throughput manner without caring the difficulties mentioned above.

5.3. Applications and Future Directions

Ultimately, a mobile miniaturized malaria rapid diagnostic kit, on chip or on board, is the most favored application. To be practical, massive parallelism has to be adopted to diagnose early when the fraction of infected RBC is only 0.0001% or less within an hour or a few minutes. The kit can be partitioned to reduce the chip waste as one part is disposable microfluidic device and the other part is diagnostic IC chip. This kind of diagnostic tool is easy to be transported to remote areas and can be effective in use since the kit does not need bulky optical equipments in diagnosis. With low power circuit design technology, the system can be powered by tiny battery or solar cell where source of electricity is limited. In these ways, electronics can reach out to people exposed to malaria but lacking of proper medical service, and so the research contributes to the world health.

On the other hand, the EIS system can be utilized in other studies. Microfluidic EIS can target on other parasitic disease of RBC or other cells rather than RBC. Besides, supported by high speed circuitry, single cell analysis such as cell differentiation and sorting can be done in high speed manner. Since EIS can provide new parameter additional to optical information in biological cell analysis, it can also get rid of the need for optical equipment.

Chapter 6 References

[1] World Health Organization. (2010, World malaria report : 2010.

[2] International Medical Corps. (2010, Fast facts on malaria. pp. 1.

[3] World Health Organization. (2010, Malaria fact sheet no.94.

[4] T. Hanscheid, "Diagnosis of malaria: a review of alternatives to conventional microscopy," Clin. Lab. Haematol., vol. 21, pp. 235-245, Aug, 1999.

[5] D. J. Sullivan, "Hemozoin: a Biocrystal Synthesized during the Degradation of Hemoglobin," 2005.

[6] Y. Park, M. Diez-Silva, G. Popescu, G. Lykotrafitis, W. Choi, M. S. Feld and S. Suresh, "Refractive index maps and membrane dynamics of human red blood cells parasitized by Plasmodium falciparum," Proceedings of the National Academy of Sciences, vol. 105, pp. 13730-13735, September 16, 2008.

[7] S. Hackett, J. Hamzah, T. M. Davis and T. G. St Pierre, "Magnetic susceptibility of iron in malaria-infected red blood cells," Biochim. Biophys. Acta, vol. 1792, pp. 93-99, Feb., 2009.

[8] C. Ribaut, K. Reybier, O. Reynes, J. Launay, A. Valentin, P. L. Fabre and F. Nepveu, "Electrochemical impedance spectroscopy to study physiological changes affecting the red blood cell after invasion by malaria parasites," Biosensors and Bioelectronics, vol. 24, pp. 2721-2725, 4/15, 2009.

[9] H. Morgan, T. Sun, D. Holmes, S. Gawad and N. Green G., "Single cell dielectric spectroscopy," J. Phys. D, vol. 40, pp. 61, 2007.

[10] H. E. Ayliffe, A. B. Frazier and R. D. Rabbitt, "Electric impedance spectroscopy using microchannels with integrated metal electrodes," Microelectromechanical Systems, Journal of, vol. 8, pp. 50-57, 1999.

[11] K. Kirk, "Membrane Transport in the Malaria-Infected Erythrocyte," Physiological Reviews, vol. 81, pp. 495-537, Apr., 2001.

[12] T. Sun , C. van Berkel, N. Green and H. Morgan, "Digital signal processing methods for impedance microfluidic cytometry," Microfluidics and Nanofluidics, pp. 179-187, Feb., 2009.

[13] L. I. Segerink, A. J. Sprenkels, P. M. ter Braak, I. Vermes and d. B. van, "On-chip determination of spermatozoa concentration using electrical impedance measurements," Lab Chip, vol. 10, pp. 1018-1024, 2010.

[14] A. Valero, T. Braschler and P. Renaud, "A unified approach to dielectric single cell analysis: Impedance and dielectrophoretic force spectroscopy," Lab Chip, vol. 10, pp. 2216-2225, 2010.

[15] Datasheet, "AD5933: 1 MSPS, 12 Bit Impedance Converter Network Analyzer (Online). Available at http://www.analog.com/static/imported-files/data_sheets/AD5933.pdf."

[16] User Manual, "XEM3001v2 User's Manual (Online). Available at http://www.opalkelly.com/library/XEM3001v2-UM.pdf."

[17] User Manual, "FrontPanel (Online). Available at http://www.opalkelly.com/library/FrontPanel-UM.pdf."

[18] H. Bow, I. V. Pivkin, M. Diez-Silva, S. J. Goldfless, M. Dao, J. C. Niles, S. Suresh and J. Han, "A microfabricated deformability-based flow cytometer with application to malaria," Lab Chip, vol. 11, pp. 1065-1073, 2011.

[19] I. W. Sherman, "Biochemistry of Plasmodium (malarial parasites)," Microbiol. Rev., vol. 43, pp. 453-495, Dec., 1979.

[20] T. Sun and H. Morgan, "Single cell microfluidic impedance cytometry – a review," Microfluidics and Nanofluidics, vol. 8, pp. 423-443, 2010.

[21] W. H. Coulter, "High speed automatic blood cell counter and cell analyzer", Proc. Nat. Electron. Conf., vol. 12, p.1034, 1956.

[22] S. P. Desai, B. M. Taff and J. Voldman, "A Photopatternable Silicon for Biological Applications," Langmuir, vol. 24, pp. 575-581, Jan., 2008.

[23] http://en.wikipedia.org/wiki/Phosphate_buffered_saline

[24] R. W. DeBlois and C. P. Bean, "Counting and Sizing of Submicron Particles by the Resistive Pulse Technique," Rev. Sci. Instrum., vol. 41, pp. 909-916, Jul, 1970.

[25] User Manual, "Agilent Impedance Measurement Handbook: A guide to measurement technology and techniques, 4th ed. (Online). Available at http:// cp.literature.agilent.com/litweb/pdf/5950-3000.pdf."